Platinum(II) olefin hydroarylation catalysts: tuning selectivity for the anti-Markovnikov product
Tandem catalytic ester hydrogenation and deoxygenation of polyethylene terephthalate

Marie Clement

A thesis

submitted in partial fulfillment of the

requirements for the degree of

Masters of Science

University of Washington

2016

Committee:

Karen Goldberg

D. Mike Heinekey

Program Authorized to Offer Degree:

Department of Chemistry

University of Washington

Abstract

Platinum(II) olefin hydroarylation catalysts: tuning selectivity for the anti-Markovnikov product

Tandem catalytic ester hydrogenation and deoxygenation of polyethylene terephthalate

Marie Louise Clement

Chair of the Supervisory Committee:
Nicole A. Boand Endowed Professor of Chemistry Karen I. Goldberg
Department of Chemistry

Pt^{II} complexes bearing unsymmetrical pyridyl-pyrrolide ligands are shown to catalyze the hydroarylation of unactivated alkenes with high selectivity for the anti-Markovnikov product. Substitution on the pyrrolide portion of the ligand allows for effective tuning of the selectivity to anti-Markovnikov alkylarene products while substitution on the pyridyl portion can promote competitive alkenylarene production.

Polyethylene Terephthalate (PET) is a widely utilized plastic, but there is growing concern about the environmental impacts of the accumulation and fragmentation of plastics into the environment. We propose an alternative to current PET recycling methods by the use of a tandem homogeneous catalytic system.

Table of Contents

List of Figures…… ii

Chapter 1: Platinum(II) olefin hydroarylation catalysts: tuning selectivity for the anti-Markovnikov product…….. 1

Introduction…… 1
1.1 Hydroarylation with neutral Pt^{II}(N-N)catalysts…… 2
1.2 Preliminary screening of potential hydroarylation complexes…….. 13
Experimental…….. 15

Chapter 2: Tandem catalytic ester hydrogenation and deoxygenation of polyethylene terephthalate…….. 46

Introduction…… 46
2.1 Ester Hydrogenation…….. 49
2.2 PET hydrogenation with 1…….. 51
2.3 PET hydrogenation with reported ester hydrogenation catalysts…… 52
2.4 Alcohol deoxygenation…….. 56
2.5 Summary…….. 58

List of Figures

1.1 Friedel-Crafts alkylation

1.2 Precatalysts employed for hydroarylation experiments.

1.3 POV-Ray thermal ellipsoid diagram of 1

1.4 POV-RAY thermal ellipsoid diagram of 3

1.5 POV-RAY thermal ellipsoid diagram of 4

1.6 POV-Ray thermal ellipsoid diagram of 5

1.7 Plot of TON for the total products generated using 1 at different concentrations of propylene.

1.8 Proposed hydroarylation catalytic cycle.

1.9 Steric interaction of olefin and ligand in the catalyst active site.

1.10 Additional precatalyst structures

1.11 ^{1}H NMR spectrum of (pypyr)PtMe(SMe_2) in C_6D_6 at 298 K.

1.12 COSY spectrum of (pypyr)PtMe(SMe_2) in C_6D_6 at 298 K.

1.13 ^{1}H NMR spectrum of (pypyr)PtPh(SMe_2) in THF-d_8 at 298K.

1.14 COSY spectrum of (pypyr)PtPh(SMe_2) in THF-d_8 at 298K.

1.15 ^{1}H NMR spectrum of ^{Me}pypyr–H in C_6D_6 at 298 K.

1.16 ^{1}H NMR spectrum of (^{Me}pypyr)PtPh(SMe_2) in C_6D_6 at 298 K.

1.17 COSY spectrum of (^{Me}pypyr)PtPh(SMe_2) in C_6D_6 at 298 K.

1.18 1D NOE spectra of (^{Me}pypyr)PtPh(SMe_2) in C_6D_6 at 298 K.

1.19 ^{1}H NMR spectrum of (py-ph-pyr)PtPh(SMe_2) in C_6D_6 at 298 K.

1.20 ^{1}H NMR spectrum of (3,3-dimethyl)butylbenzene in $CDCl_3$ at 298 K.

1.21 ^{1}H NMR spectrum of α -*t*.butylstyrene in $CDCl_3$ at 298 K.

1.22 ^{1}H NMR spectra (C_6D_6) for thermolysis of (pypyr)PtPh(SMe_2) (**3**).

1.23 ^{1}H NMR spectra (C_6D_6) for of (^{Me}pypyr)PtPh(SMe_2) (**4**).

1.24 POV-Ray diagram of **1** shown with thermal ellipsoids at the 50% probability level.

1.25 POV-Ray diagram of **3** shown with thermal ellipsoids at the 50% probability level.

1.26 POV-Ray diagram of **4** shown with thermal ellipsoids at the 50% probability level.

1.27 POV-Ray diagram of **5** shown with thermal ellipsoids at the 50% probability level.

2.1 Traditional synthesis route of PET

2.2 Proposed PET cycle

2.3 Catalytic depolymerization of PET with Milstein's Ru(PNN) complex.

2.4 Hydrogenation of ethyl benzoate.

2.5 ^{1}H NMR spectrum of ethyl benzoate hydrogenation with **1**.

2.6 Proposed catalytic cycle for the hydrogenation and deoxygenation of PET

2.7 Previously reported ester hydrogenation catalysts were screened in this work.

2.8 ^{13}C NMR spectrum of PET hydrogenation with **4**.

2.9 ^{13}C NMR spectrum of PET hydrogenation with **4** at 40, 65, and 80 atm of H_2.

2.10 Ir(POCOP) deoxygenation complexes

2.11 ^{13}C NMR spectrum of benzyl alcohol deoxygenation with **4**.

2.12 Proposed catalytic cycle for the hydrogenation of BDM.

2.13 Ir(PCP) (left) and [Cp*Ir(bipy)H]OTf (left) catalyst

2.14 Other polyesters and polycarbonates to trial

Introduction:

Efficient catalytic anti-Markovnikov hydroarylation of olefins would provide an atom efficient route to linear alkyl benzenes directly from terminal olefins and benzene (**A**, Figure 1.1).[1] Traditional Friedel-Crafts catalysts (e.g. $AlCl_3$ or HF) produce the branched, Markovnikov alkylarene products (**B**, Figure 1.1).[2] Recently, several homogeneous transition metal catalysts have been reported that demonstrate moderate selectivity to the linear alkyl anti-Markovnikov products (**A**).[3]

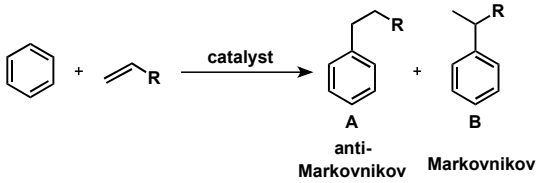

Figure 1.1. Friedel-Crafts alkylation

Studies of anti-Markovnikov/Markovnikov (**A/B**) selectivity in hydroarylation reactions of unactivated alkenes have been reported primarily using propylene and benzene as substrates with Ir, Ru or Pt catalysts. The Ir^{III} complexes, $Ir(acac–O,O)_2(R)(L)$ (R = (acac–C^3) or Ph, L = H_2O, pyridine) favored the anti-Markovnikov product with an **A:B** ratio of 61:39.[3] A similar ratio was obtained with the Ru^{II} system, TpRu(CO)(NCMe)(Ph) (Tp = trispyrazolylborate).[4] In contrast, reported Pt^{II} based catalysts for olefin hydroarylation have produced much lower selectivities with respect to anti-Markovnikov products. With the Pt^{II}–bipy cationic complex, [(^{t}bpy)Pt(Ph)(THF)][BAr'$_4$], (^{t}bpy = 4,4'-di-*tert*-butyl-2,2'- bipyridyl, Ar' = 3,5-bis (trifluoromethyl)phenyl) as a precatalyst, a ratio of 34:66 **A:B** was found favoring the Markovnikov product.[5] When 1-pentene was used as the olefin, a similar selectivity of 32:68 for **A:B** was observed.[6] Optimization of the Pt–bipyridyl

system through modification of the ligand was of limited success. The related Pt^{II} complex, [(dpm)Pt(Ph)(THF)][BAr'$_4$], (dpm = 2,2'-dipyridylmethane) produced a higher turnover number (TON) for ethylbenzene production, but showed reduced activity for hydroarylation of longer chain α-olefins than the [(^{t}bpy)-Pt(Ph)(THF)][BAr'$_4$] precatalyst. [7] The [(dpm)Pt(Ph)(THF)][BAr'$_4$] system also underperformed with respect to selectivity for the anti-Markovnikov product with propylene and benzene (**A:B** 23:77).[6]

An **A:B** ratio in favor of the Markovnikov product (15:85) was reported when the neutral Pt^{II} complex (py^{Me2}pyr)PtPh(SMe_2), (py^{Me2}pyr = 3,5-dimethyl-2-(2-pyridyl) pyrrolide (**1**)) was used as a precatalyst for propylene hydroarylation with benzene. [8] We found that modification of the precatalyst through varying substituents on the unsymmetrical (pyridyl)pyrrolide ligands is highly effective in tuning the **A:B** ratio in these neutral Pt^{II} systems. [9]

1.1 Hydroarylation with neutral Pt^{II}(N-N)catalysts:

The Pt^{II} complexes specifically shown in Figure 1.2 were employed as precatalysts for the reaction of a range of olefins and benzene to produce alkylarenes. Complexes **1** – **5** show significant differences in the ratio of anti-Markovnikov (**A**) to Markovnikov (**B**) products. Additionally, the amount of alkylarene product generated versus a side reaction leading to an alkenylarene product was dependent on the substituents on the (pyridyl)pyrrole ligand.

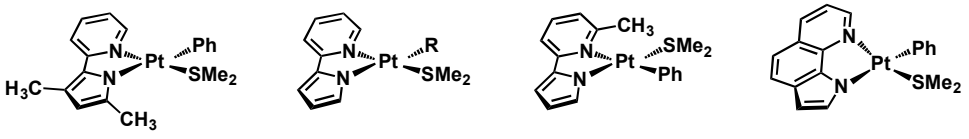

(1) (2) R = CH_3 (3) R = Ph (4) (5)

Figure 1.2 Precatalysts employed for hydroarylation experiments.

Complex **1,** previously shown to be a competent precatalyst for olefin hydroarylation,[8] was recently characterized by X-ray crystallography (XRD) (Figure 1.3).[10] It is notable that the SMe_2 ligand is located *trans* to the pyridyl group in the square planar configuration of **1**. This geometrical arrangement is significant, as the regioselectivity of the hydroarylation product (Markovnikov or anti-Markovnikov) is determined by the migration of the phenyl group to the olefin (*vide infra*). Substitution of SMe_2 by the olefin substrate should place the olefin *trans* to the pyridyl group and *cis* to the pyrrolide.[11]

It is reasonable to hypothesize that the methyl group on the pyrrolide could be influencing the regioselectivity of the migratory insertion step. Thus, we sought to investigate a similar complex with an unsubstituted pyrrolide group, pypyr = 2-(2-pyridyl)pyrrolide, complex **3** (Figure 1.4). Significant differences were noted in the attempted synthesis of **3** by a route similar to that used to prepare **1**. In the preparation of **1**, the reaction of the platinum dimer $[PtMe_2(SMe_2)]_2$[12] with $py^{Me2}pyr$–H resulted in N–H bond cleavage and release of methane. C–H activation of the benzene solvent also occurred in this reaction and within 30 minutes at room temperature, **1** was produced along with a second equivalent of methane. When the same procedure was followed with pypyr–H, C–H activation of the benzene solvent was either not observed at all or did not proceed to completion. Depending on the reaction conditions, the Pt^{II} methyl complex (pypyr)$PtMe(SMe_2)$ (**2**) or a mixture of **2** and the Pt^{II} phenyl complex (pypyr)$PtPh(SMe_2)$ (**3**) were formed.[10] Complex **2** was characterized by a singlet in the ^1H NMR spectrum attributed to the Pt–Me group at

1.33 ppm ($^2J_{PtH}$ = 79.7 Hz). Mild heating of a benzene solution of **2** did not result in full conversion to **3**, and accessing temperatures above 60 °C resulted in formation of Pt black.

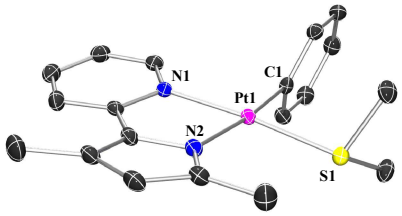

Figure 1.3 POV-Ray thermal ellipsoid diagram of **1** at the 50% probability level. Hydrogen atoms omitted for clarity. Selected bond lengths (Å) and angles (°) for **1**: C1–Pt1 = 2.0131(17), N1–Pt1 = 2.0538(15), N2–Pt1 = 2.0888(15), S1–Pt1 = 2.2606(6), C1–Pt1–N1 = 93.12(6), C1–Pt1–N2 = 172.74(6), C1–Pt1–S1 = 90.51(5), N1–Pt1–N2 = 79.63(6), N1–Pt1–S1 = 174.99(4), N2–Pt1–S1 = 96.75(4).

Complex **3**, the direct Pt^{II} phenyl analog of **1** bearing the pypyr ligand, was instead prepared by the reaction of pypyr–H with the Pt^{II} phenyl starting material $[PtPh_2(SMe_2)]_2$.[13] The ^{1}H NMR spectrum of (pypyr)PtPh(SMe_2) (**3**) in C_6D_6 contains a singlet at 2.30 ppm ($^3J_{PtH}$ = 59.6 Hz) assigned to the dimethyl sulfide group bound to platinum. An XRD study on a single crystal of **3** revealed a square planar Pt^{II} complex, with the phenyl ligand again positioned *trans* to the pyrrole group as was observed for **1** (Figure 1.4). The bond lengths and bond angles within **1** and **3** are similar.[10]

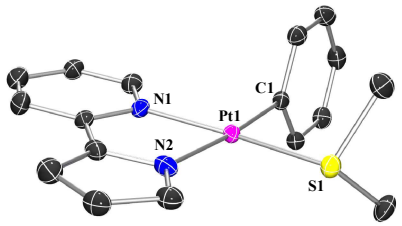

Figure 1.4 POV-RAY thermal ellipsoid diagram of **3** at the 50% probability level. Hydrogen atoms omitted for clarity. Selected bond lengths (Å) and angles (°) for 3: C1–Pt1 = 2.015(2), N1–Pt1 = 2.047(2), N2–Pt1 = 2.068(2), S1–Pt1 = 2.2490(6), C1–

Pt1–N1 = 94.44(9), C1–Pt1–N2 = 173.81(9), C1–Pt1–S1 = 93.32(7), N1–Pt1–N2 = 79.48(8), N1–Pt1–S1 = 172.07(6), N2–Pt1–S1 = 92.72(6).

The influence of a methyl group in the ortho position of the pyridyl ring of the ligand was also examined. Reaction of $[PtPh_2(SMe_2)]_2$ with 6-methyl-2-(1H-pyrrol-2-yl)pyridine (^{Me}pypyr-H) led to clean formation of (^{Me}pypyr)PtPh(SMe_2) (**4**). The ^{1}H NMR spectrum of **4** in C_6D_6 contains upfield singlets at 2.30 ppm ($^3J_{PtH}$ = 50.1 Hz) and 2.32 ppm assigned to the platinum bound dimethyl sulfide and the methyl group attached to the pyridine ring, respectively. An XRD study revealed that, in contrast to the structures of **1** and **3**, the phenyl ligand in **4** is situated *trans* to the pyridyl moiety (Figure 1.5). Close proximity of the pyridyl ring to the dimethyl sulfide was corroborated by 1D NOE NMR spectroscopy, indicating that the solution structure is similar to that found in the solid state.[10]

Thermolysis of **4** in C_6D_6 for up to 200 hours at 100 °C did not result in any isomerization to the isomer with the phenyl group *trans* to the pyrrolide moiety.[10] In contrast, heating a solution of **1** in C_6D_6 at 100 °C resulted in partial conversion to the isomer with the phenyl group *trans* to the pyridyl ring. A ratio of more than 2:1 favoring the isomerized species after 133 hours was observed.[8] Similarly, heating **3** in C_6D_6 for up to 200 hours at 100 °C produced a mixture of isomers in a ratio of 1.23:1 favoring the isomer with the Pt–phenyl *trans* to the pyridyl group.

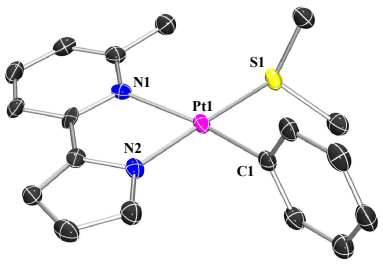

Figure 1.5 POV-RAY thermal ellipsoid diagram of **4** at the 50% probability level. Hydrogen atoms omitted for clarity. Selected bond lengths (Å) and angles (°) for 4: C1–Pt1 = 1.994(5), N1–Pt1 = 2.220(4), N2–Pt1 = 2.002(4), S1–Pt1 = 2.2736(13), C1–Pt1–N1 = 168.98(17), C1–Pt1–N2 = 90.47(18), C1–Pt1–S1 = 89.37(14), N1–Pt1–N2 = 78.81(16), N1–Pt1–S1 = 101.44(11), N2–Pt1–S1 = 177.76(12).

Complex **5**, another Pt^{II} phenyl analog of **1** and **3** has a fused ring structure that is similar to the pypyr ligand. It was prepared by the reaction of 1H-Pyrrole[3,2-h]quinolone[14] (py-ph-pyr–H) with the Pt^{II} phenyl starting material $[PtPh_2(SMe_2)]_2$.[15] The ^1H NMR spectrum of (py-ph-pyr)$PtPh(SMe_2)$ (**5**) in C_6D_6 contains a singlet at 1.68 ppm ($^3J_{PtH}$ = 61.3 Hz) assigned to the dimethyl sulfide group bound to platinum. An XRD study on a single crystal of **5** revealed a square planar Pt^{II} complex, with the phenyl ligand again positioned *trans* to the pyrrole group as was observed for **1** (Figure 1.6).

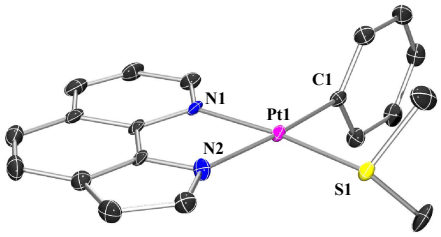

Figure 1.6 POV-Ray thermal ellipsoid diagram of **5** at the 50% probability level. Hydrogen atoms omitted for clarity. Selected bond lengths (Å) and angles (°) for **5**: C1–Pt1 = 2.002(5), N1–Pt1 = 2.079(4), N2–Pt1 = 2.113(4), S1–Pt1 = 2.2443(12), C1–Pt1–N1 = 92.82(17), C1–Pt1–N2 = 174.56(17), C1–Pt1–S1 = 93.79(13), N1–Pt1–N2 = 81.75(15), N1–Pt1–S1 = 173.09(12), N2–Pt1–S1 = 91.65(12).

Complexes **1**–**5** were tested as precatalysts for hydroarylation with propylene, 1-hexene, and neohexene (3,3-dimethyl-1-butene) at 100 °C. Reactions were monitored *in situ* by ^1H NMR spectroscopy with yields and TON determined after either 120 or 240 hours using gas chromatography (Table 1).

As can be seen by comparing entries 1, 2 and 4 in Table 1, the removal of the methyl groups from the pyrrolide portion of the ligand led to a striking change in the anti-Markovnikov (**A**) to Markovnikov (**B**) selectivity for the hydroarylation of propylene. With complex **1**, the Markovnikov product was strongly favored (**A**:**B** ratio of 15:85). Utilizing complexes **2** or **3**, under the same reaction conditions, the products **A** and **B** were formed in a 48:52 ratio, representing a significant increase in the anti-Markovnikov selectivity. An even higher **A**:**B** ratio of 57:43 was achieved when a fused ring structure (complex 5) was used. Monitoring the hydroarylation reactions for *n*-propylbenzene by ^{1}H NMR spectroscopy revealed that the selectivity (**A**:**B** ratio) was conserved over time (120 h) when complexes **1**, **2**, **3**, and **5** were used as precatalysts.[16]

While removing the methyl group on the pyrrolide ring led to a significant increase in the selectivity for the anti-Markovnikov product, it also resulted in ca. 40% lower TON (entries 1 and 4). This difference may be related to the decreased electron density at platinum leading to a lower propensity for oxidative addition of the arene C–H bond. This would be consistent with the catalyst synthesis results wherein the phenyl complex **1** was formed directly from the reaction of py^{Me2}pyr–H with $[PtMe_2(SMe_2)]_2$ in benzene, but the corresponding reaction with pypyr–H primarily yielded only the Pt–Me complex, **2**. However, it could also be an indication of reduced catalyst lifetime of **3** compared to **1**.

Remarkably, increasing the propylene concentration increased the TON to a level that was comparable to that observed when precatalyst **1** was used in place of precatalyst **3**. As shown in entries 3–5, increasing the propylene concentration

resulted in higher TON for the hydroarylation reaction with precatalyst **3**. The reactions shown in entries 3–5 were monitored by ^{1}H NMR spectroscopy, and the similar initial slopes in the plots of TON vs. time suggests that the increased TON with increased olefin concentration results in large part from greater catalyst longevity. As shown in Figure 1.7, the TON begins to plateau at longer reaction times with higher olefin concentration.

When 1-hexene was used as the substrate for the hydroarylation reaction, a comparable product ratio (16:83 for **A**:**B**, entry 8) to that obtained with propylene was observed with complex **1** as the precatalyst. In contrast, with catalyst **3** (entry 9), the anti-Markovnikov selectivity is enhanced to the extent that it becomes the favored product with an **A**:**B** ratio of 57:43. With 1-hexene, increasing the olefin concentration past 0.5 M had little effect on the TON. For example, when a three-fold increase to 1.6 M was employed with complex **3** as the precatalyst, a similar TON was measured (entries 9 and 12).

Table 1 Hydroarylation TON and ratio of products.[a],[b]

entry	precatalyst	olefin	M olefin	TON[c]	**A**:**B**:**C**[d],[e]
1	**1**	propylene	0.54	17.9 (0.9)	13:84:3
2	**2**	propylene	0.54	10.4 (0.7)	48:52:0
3	**3**	propylene	0.26	9.3 (0.8)	47:53:0
4	**3**	propylene	0.54	10.7 (0.9)	48:52:0
5	**3**	propylene	0.80	15.5 (0.3)	49:51:0
6	**4**	propylene	0.54	2.7 (0.1)	3:17:80[g]
7	**5**	propylene	0.54	3.8 (0.2)	57:43:00
8	**1**	1-hexene	0.51	11.8 (1.1)	16:83:1
9	**3**	1-hexene	0.51	8.4 (0.2)	57:43:0
10	**3**	1-hexene	0.51[f]	11.7 (0.8)	57:43:0
11	**3**	1-hexene	1.6	9.0 (1.5)	59:41:0
12	**3**	1-hexene	1.6[f]	10.5 (0.6)	58:42:0
13	**5**	1-hexene	0.51	5.1 (0.2)	61:36:02
14	**1**	neohexene	0.51	2.5 (0.2)	15:48:37
15	**3**	neohexene	0.51	3.1 (0.1)	85:5:10

16	**3**	neohexene	2.6	11.8 (0.2)	90:9:1
17	**5**	neohexene	0.51	1.7 (0.04)	95:04:01

[a] Experimental conditions: 0.1–1.0 mmol olefin, 1.3 mol% catalyst, excess C_6H_6, 100 °C, 120 hours, unless otherwise noted. [b] Experiments were conducted 2–4 times and averaged. [c] Standard Deviation noted in parentheses [d] C = product of branched β-hydride elimination [e] Standard deviations for these values were all less than 1 and averaged 0.4. [f] Reaction time of 240h [g] A large amount of disubstituted product was observed. A ratio of **A:B:C:D** = 1:10:45:44 was calculated. TON is for monosubstituted product.

When the significantly bulkier olefin neohexene was used as the substrate, selectivity for the anti-Markovnikov product drastically increased to a ratio of 85:5 for **A**:**B** using **3** (entry 13). An additional product, the branched β-hydride elimination product (**C**), which in this case was α-tert-butylstyrene, was also observed comprising 10% of the hydroarylated product. While selectivity for the anti-Markovnikov product was high, the TON was quite limited. Increasing the olefin concentration by five-fold (from 0.5 M to 2.6 M, entries 15 and 16) however, led to a four-fold increase in TON. The β-hydride elimination pathway was inhibited and the **A**:**B** selectivity was measured at 90:9.

As decreasing the steric bulk on the pyrrolide side of the ligand had such a significant influence on selectivity of olefin hydroarylation, the effect of a methyl group on the pyridyl side was also examined. Notably, this small ligand variation changed the major product of the propylene reaction from alkylarene to α-methyl styrene[17] (80% of the monosubstituted arene product). Di-substituted products **D**, were also observed in this reaction and accounted for ca. 44% of the total hydroarylation products by GC analysis. A low TON for monosubstituted products of 2.7 was recorded for this reaction.

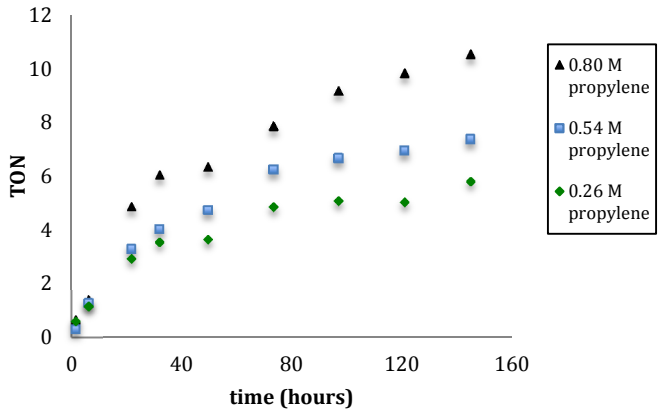

Figure 1.7 Plot of TON for the total products generated using **1** at different concentrations of propylene. Experimental conditions: 0.5-2.6 M olefin, 1.3 mol% catalyst, excess C_6H_6, 100 °C.

Several mechanisms have been proposed for Pt^{II} hydroarylation.[18,19,20,8] Results with catalysts **1**–**3**, **5** and olefin substrates ethylene, propylene, 1-hexene, and neohexene are consistent with the catalytic cycle shown in Figure 1.8. Migration of the phenyl group to the olefin generates an alkyl arene ligand and an open site at the metal center. Previously reported deuterium labeling studies in the hydroarylation of ethylene with the ($py^{Me2}pyr$)PtPh(SMe_2) system[8] indicate that an intramolecular C–H activation of the arene ring occurs next, followed by alkyl C–H reductive elimination.[8] Intermolecular C–H activation of arene solvent is then followed by reductive coupling to generate the coordinated alkyl arene product. Substitution of the coordinated arene with olefin then closes the cycle.[8]

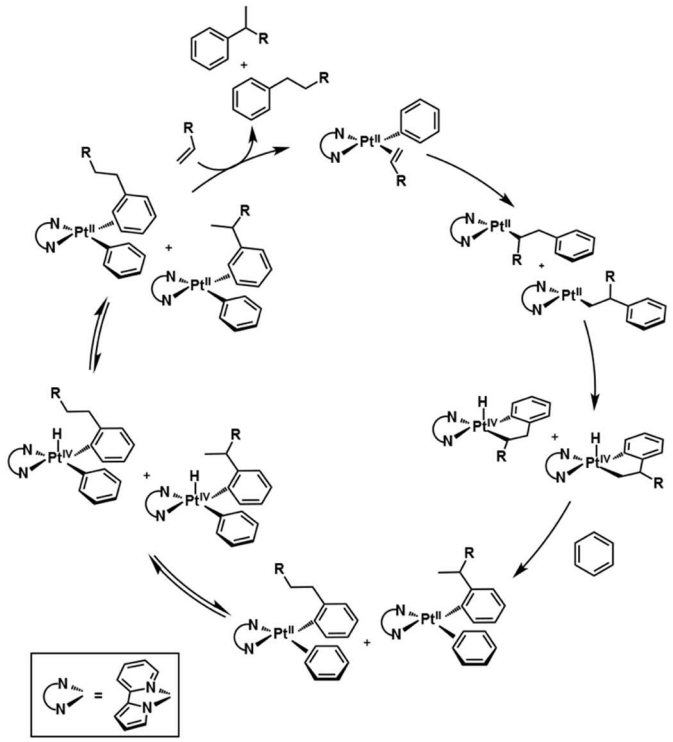

Figure 1.8 Proposed hydroarylation catalytic cycle.

As depicted in Figure 1.9, migration of the phenyl group to the olefin is proposed as the Markovnikov/anti-Markovnikov selectivity determining step. To allow for proper orbital overlap for this migration, the two carbons of the olefin need to be in the plane of the square planar Pt^{II} complex. As shown in Figure 1.9, there are two possible rotamers for this configuration. A methyl group at the 5-position of the pyrrolide ring (precatalyst **1**) should sterically favor rotamer **b** over rotamer **a**. The methyl group on the pyrrolide ring could also affect the relative insertion barriers (k_b versus k_a). If the rotamers are interconverting rapidly, the reaction leading to either the branched or linear product would be under Curtin-Hammett conditions with the **A**:**B** ratio equal to $K_{a/b}(k_a/k_b)$. Thus with precatalyst **1** and propylene, the sterics of the 5-Me group on the pyrrolide favor the branched product while with precatalyst **3** and propylene, approximately equal amounts of **A**

and **B** are observed. As the sterics of the olefin increases (propylene<1-hexene<<neohexene), the effects on the relative energetics of the rotamers and the relative insertion barriers result in higher amounts of anti-Markovnikov product when precatalyst **3** is used. Notably, steric crowding of the *n*-alkyl chain or *t*-Bu group with the phenyl group on Pt may favor rotamer **a**, but the steric interactions are also likely to inhibit phenyl migration to the more substituted carbon. An alternative explanation for olefin hydroarylation selectivity was offered with respect to a related Pt^{II} system bearing a symmetric bipyridyl ligand.[6] Reversible migratory insertion of the phenyl group and the olefin was proposed to be followed by irreversible intermolecular C–H activation to yield the branched and linear products. A similar explanation may also be applicable here and computational studies could provide further insight.

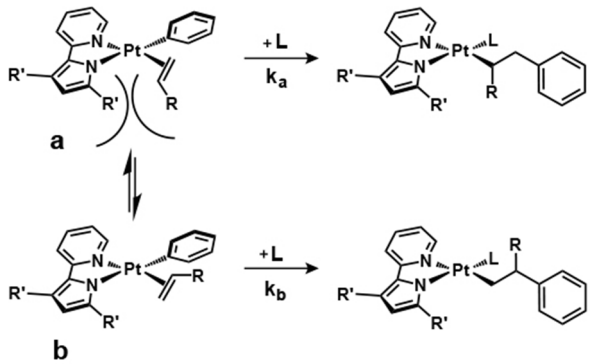

Figure 1.9 Steric interaction of olefin and ligand in the catalyst active site. R = H, CH_3, C_5H_{11}, *t*Bu, R' = H, CH_3

When **4** is used as the precatalyst for the reaction of propylene with benzene, α-methyl styrene is the primary product, rather than alkylarenes. A notable difference between **4** and the precatalysts **1** and **3** is the orientation of the Ph group. The phenyl group is *trans* to the pyrrolide in **1** and **3** and *trans* to the pyridyl group in **4**. Migratory insertion of the phenyl group to an olefin residing in the place of the

SMe_2 group would then yield an alkyl aryl group *trans* to the pyrrolide for **4**. β-Hydride elimination may then be favored over C–H activation from this configuration leading to α-methyl styrene. It is also possible that the three-coordinate species formed after phenyl migration isomerizes and the methyl group in the 6-position on the pyridyl ring inhibits approach of the arene. In this case, β-hydride formation could be kinetically favored over intramolecular arene C–H activation.

1.2 Preliminary screening of other potential pre-catalysts for olefin hydroarylation:

Additional complexes were synthesized and screened for olefin hydroarylation catalytic activity (Figure 1.10). Complex **6** was chosen to determine if altering the (pyridyl)pyrrolide structure of the ligand to 2-phenylpyridine would increase the linear selectivity. It is still a neutral square planar Pt^{II} structure, but with a potentially more crowded active site. However, when **6** was screened for hydroarylation with propylene at 100 °C almost no activity was observed and a large amount of Pt black was formed.

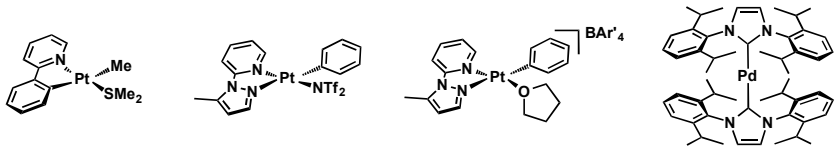

Figure 1.10: Additional precatalyst structures

High TON for the products of hydroarylation have been reported for similar cationic Pt complexes.[19] Based on this, we synthesized complexes **7** and **8**. The cationic structure of 7 and 8 bear resemblance to the Gunnoe bipy system,[5 - 7] but do not have the same symmetric bipy backbone. These complexes were chose as we were

interested in exploring how removing the symmetry of the precatalysts backbone would effect selectivity for the linear alkylbenzene. However, the initial screenings of these complexes were found to have **A**:**B**:**C** ratios of 12:84:4 and 21:41:38 respectively, which is similar to the selectivity observed by the Gunnoe group.[6] Since a decreased linear selectivity in comparison to the neutral Pt- pyridyl-pyrrolide pre-catalysts was observed in the initial screening, **7** and **8** were not pursued further.

Complex **9** was inspired by the $Ni(IPr)_2$ N-heterocyclic carbene complex reported by the Hartwig group, IPr = N,N'-(2,6-Diisopropylphenyl)dihydroimidazolium. An **A**:**B** ratio of >95:5 was reported for this complex with 1-octene as the olefin and benzene as the arene.[21] **9** showed some initial promise when the active catalyst was generated *in situ* from $Pd_2(dba)_3$ and IPr·HCl. A very small amount of linear product, and a lot of catalyst decomposition was observed by ^1H NMR spectroscopy. We then thought screening the isolated complex[22] would improve the stability of the catalyst and generate fewer side products. However, when the isolated complex was screened for hydroarylation neither linear nor branched products were formed. This is most likely due to the inability of the IPr ligands to dissociate from the metal center, pick up an olefin, and begin the catalytic cycle. This is different from the reactivity observed with $Ni(IPr)_2$ in which one of the IPr ligands dissociates from the metal center and an arene and olefin are bound in order to begin the catalytic cycle.[21]

In summary, the unsymmetrical nature of the pyridyl-pyrrolide ligands on Pt^{II} was used to tune the regioselectivity in homogeneous olefin hydroarylation reactions. As two sites at the metal center are required for olefin hydroarylation–

one for arene C–H activation and one for olefin coordination–a strategy wherein the two sites have different steric and electronic environments was demonstrated to provide significant advantage in increasing selectivity of the catalytic system. A selectivity of 57:43 favoring the anti-Markovnikov product was obtained with benzene and 1-hexene using an optimized catalyst. Even more dramatic, an **A**:**B** ratio of 94:6 again favoring the anti-Markovnikov product was obtained using benzene and neohexene. Notably 10% of the alkenylarene product **C** was obtained in this reaction such that the **A**:**B**:**C** ratio was 85:5:10. In addition to the high selectivities for the anti-Markovnikov products, it is notable that these unsymmetrical neutral Pt^{II} systems were not inhibited by excess olefin as was previously observed for the closely related symmetric bipyridyl Pt^{II} systems.[18] Significantly it was shown that with propylene as the substrate, higher olefin concentrations resulted in increased catalyst lifetimes. Finally, additional structures outside of the initial (pyridyl)pyrrolide ligand structure were explored for a potential hydroarylation catalyst. None of these complexes were able to achieve the linear selectivity desired for this project.

Experimental:

Synthetic Procedures and Characterization:

General: Unless it is otherwise specified, all reactions involving metal complexes were carried out under a nitrogen atmosphere in a glove box, using standard Schlenk or high vacuum line techniques. 3,5-dimethyl-2-(2-pyridyl)pyrrole ($py^{Me2}pyr$)-H,[23] ($py^{Me2}pyr$)PtPh(SMe_2), (**1**),[24] 2-(1H-pyrrol-2-yl)pyridine (pypyr)-H,[25] bis[dimethyl(μ-dimethyl sulfide)platinum(II)],[26] and bis[diphenyl(μ-dimethyl

sulfide)platinum(II)][27] 1H-Pyrrole[3,2-h]quinolone[28] were prepared using previously reported literature procedures. Diethyl ether, tetrahydrofuran (THF) and pentane used in synthetic procedures were passed through two packed columns of neutral alumina. Benzene used in synthetic procedures was passed through a column of neutral alumina and a column of Q5 reagent. Deuterated solvents (benzene-d_6, tetrohydrofuran-d_8) were dried over sodium metal/benzophenone and distilled prior to use. All other reagents and solvents were used as received from their commercial suppliers unless otherwise specified. NMR spectra were recorded at 25 °C on a Bruker AV300, DRX499, AV500, or AV700 MHz spectrometer. All ^{1}H and ^{13}C NMR spectra are referenced to $SiMe_4$ (δ = 0 ppm) using the residual solvent signal as the internal standard and chemical shifts are reported in parts per million (ppm). Hexamethylbenzene (0.0012 mmol) was used as an internal standard for monitoring the ^{1}H NMR experiments. Elemental analyses were performed by the CENTC Elemental Analysis Facility in Rochester, NY, or Atlantic Microlab Inc. in Norcross, GA.

All GC-FID chromatograms were recorded with an Agilent 7890A GC instrument. A Gas-Pro Agilent porous layer open tubular (PLOT) 30 m column with a 0.320 mm diameter was used. The starting temperature was 100 °C, which was followed by a ramp of 10 °C per min until the final temperature of 269 °C was reached and held for 8 min. Calibration curves of the products were generated by serial dilutions of stock solutions in the range of 0.20 mM–0.01 mM. Mesitylene (6 μL) was used as an internal standard in order to calculate product yields and ratios.

Synthesis of (pypyr)PtMe(SMe_2) (2):

A solution of pypyr–H (21.2 mg, 0.146 mmol) in C_6H_6 (3 mL) was added dropwise to a stirring solution of $[PtMe_2(SMe_2)]_2$ (59.8 mg, 0.073 mmol) in C_6H_6 (3 mL) in a sealable reaction flask equipped with a Teflon valve. The mixture was stirred for 30 min at 25 °C. The mixture changed to a gold-yellow color, and bubbles indicating evolution of a gas were observed. The flask was then heated at 60 °C for 3 hours. After this, the solvent was removed in vacuo, which yielded a yellow powder. Recrystallization from THF/pentane at room temperature resulted in (pypyr)PtMe(SMe_2) as a yellow powder in 32% yield (19.4 mg, 0.047 mmol). ^{1}H NMR (301 MHz, C_6D_6, 298 K): δ 8.24 (d, J_{HH} = 6.1 Hz, $^3J_{PtH}$ = 17.1 Hz, 1H), 7.63 (s, $^3J_{PtH}$ = 19.0 Hz, 1H), 7.08 (d, J_{HH} = 8.2 Hz, 1H), 7.01 (dd, J_{HH} = 1.0 Hz, J_{HH} = 3.7 Hz, 1H), 6.88 (m, 1H), 6.72 (dd, J_{HH} = 2.1 Hz, J_{HH} = 3.6 Hz, $^4J_{PtH}$ = 21.6 Hz, 1H), 6.23 (m, 1H), 1.66 (s, $^3J_{PtH}$ = 49.8 Hz, 6H), 1.33 (s, $^2J_{PtH}$ = 79.7 Hz, 3H) ^{13}C{^{1}H} NMR (125 MHz, C_6D_6, 298 K): δ 158.23, 143.96, 141.20, 137.22, 130.41, 117.88, 117.64, 112.03, 110.33, 20.77, 16.91. Anal. Calcd. for $C_{13}H_{18}N_2SPt$: C, 34.70; H, 3.88; N, 6.74. Found: C, 34.57; H, 3.73; N, 6.53.

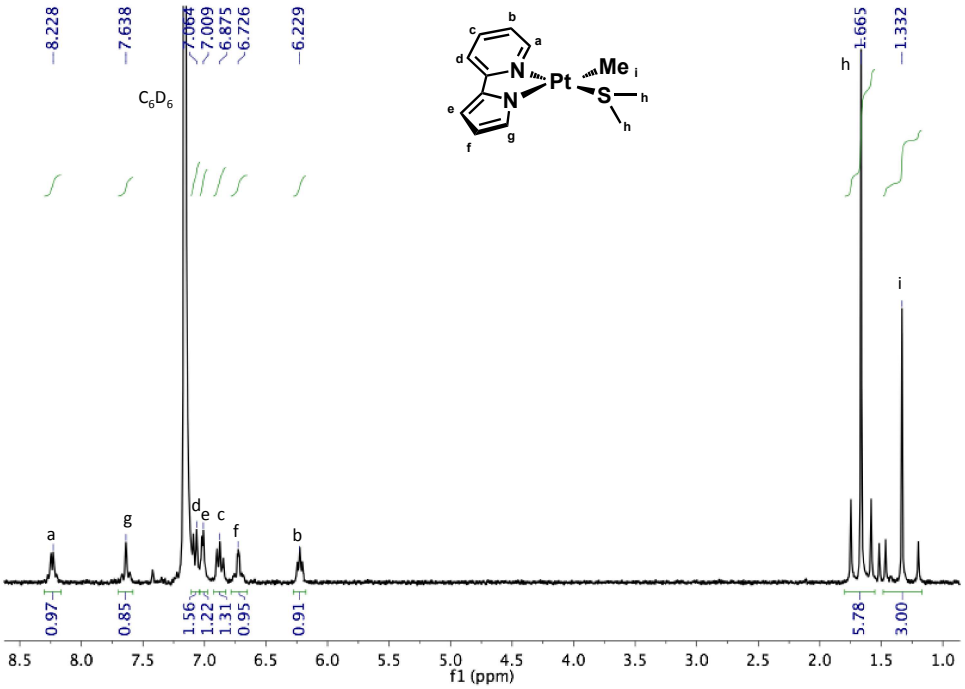

Figure 1.11 ^{1}H NMR spectrum of (pypyr)PtMe(SMe$_2$) in C_6D_6 at 298 K.

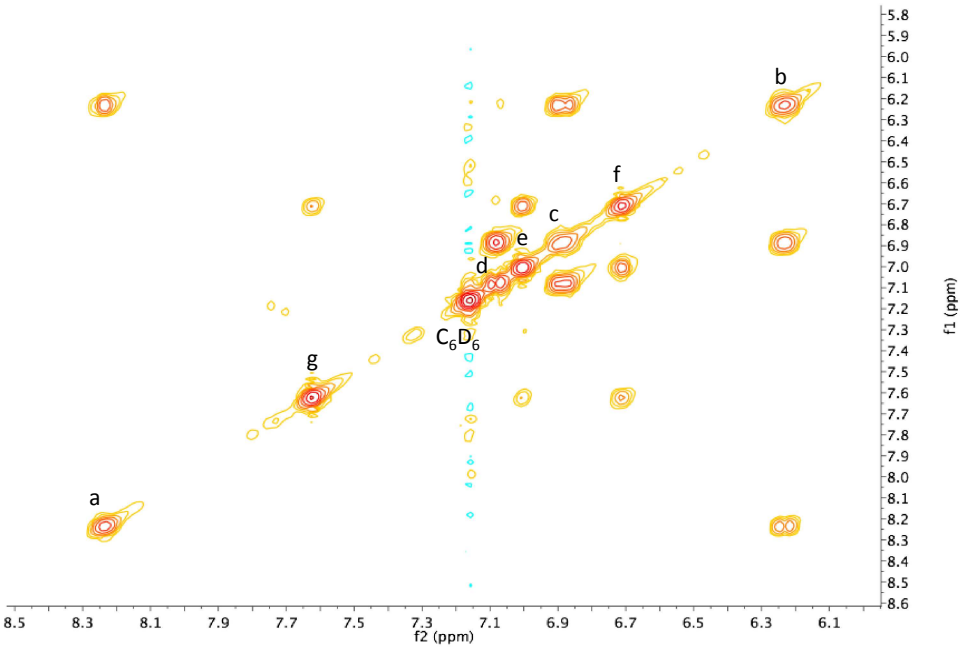

Figure 1.12 COSY spectrum of (pypyr)PtMe(SMe$_2$) in C_6D_6 at 298 K.

During one attempted synthesis of **2** from $[PtMe_2(SMe_2)]_2$ and (pypyr)-H, a mixture of both (pypyr)$PtMe(SMe_2)$ (**2**) and (pypyr)$PtPh(SMe_2)$ (**3**) in a ratio of 2:1 was observed by ^1H NMR spectroscopy.

Synthesis of (pypyr)$PtPh(SMe_2)$ (3):

A solution of pypyr–H (21.2 mg, 0.146 mmol) in C_6H_6 (3 mL) was added dropwise to a stirring solution of $[PtPh_2(SMe_2)]_2$ (59.8 mg, 0.073 mmol) in C_6H_6 (3 mL) in a Schlenk flask. The mixture was a gold/yellow color and was stirred for 2 hours at 25 °C. The solvent was removed in vacuo to yield a yellow solid. Recrystallization in THF/Et_2O resulted in (pypyr)$PtPh(SMe_2)$ as a yellow powder in 50% yield (34.7 mg, 0.073 mmol). ^1H NMR (500 MHz, THF-d_8, 298 K): δ 7.53 (m, 3H), 7.44 (m , 1H), 7.02 (m, 2H), 6.90 (m, 2H), 6.85 (m, 1H) 6.67 (dd, 1H) 6.50 (m, 1H) 6.15 (m, 1H) 2.30 (s, $^3J_{PtH}$ = 59.6 Hz, 6H) $^{13}C\{^1H\}$ NMR (125 MHz, THF-d_8, 298 K): δ 160.48, 149.55, 138.81, 138.57, 138.40, 131.33, 128.77, 123.86, 117.98, 117.80, 112.25, 110.61, 23.53. Anal. Calcd. for $C_{17}H_{18}N_2SPt$: C, 42.76; H, 3.80; N, 5.87. Found: C, 42.94; H, 3.83; N, 5.85.

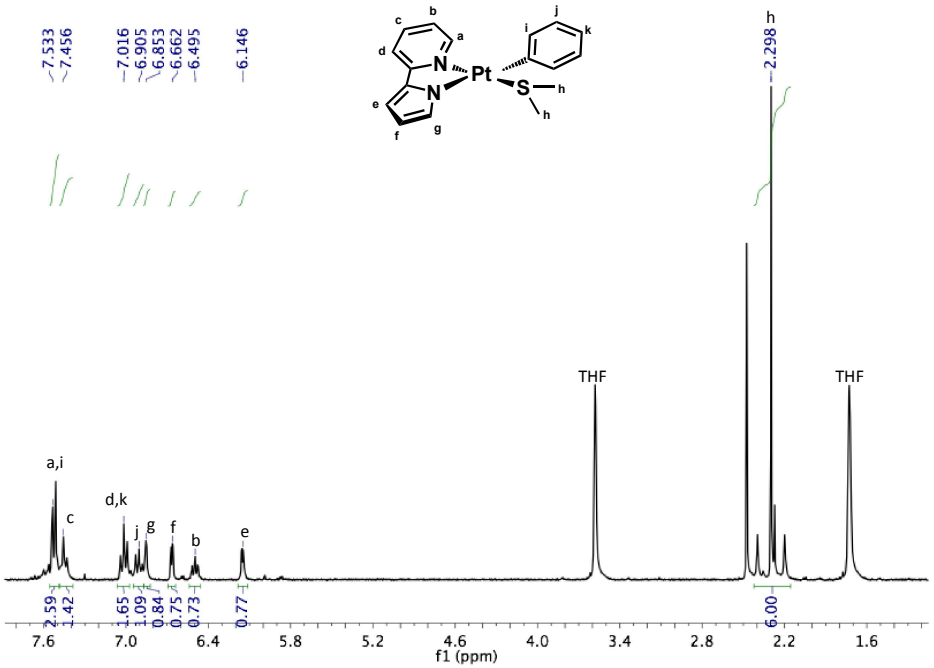

Figure 1.13 ^{1}H NMR spectrum of (pypyr)PtPh(SMe$_2$) in THF-d_8 at 298K.

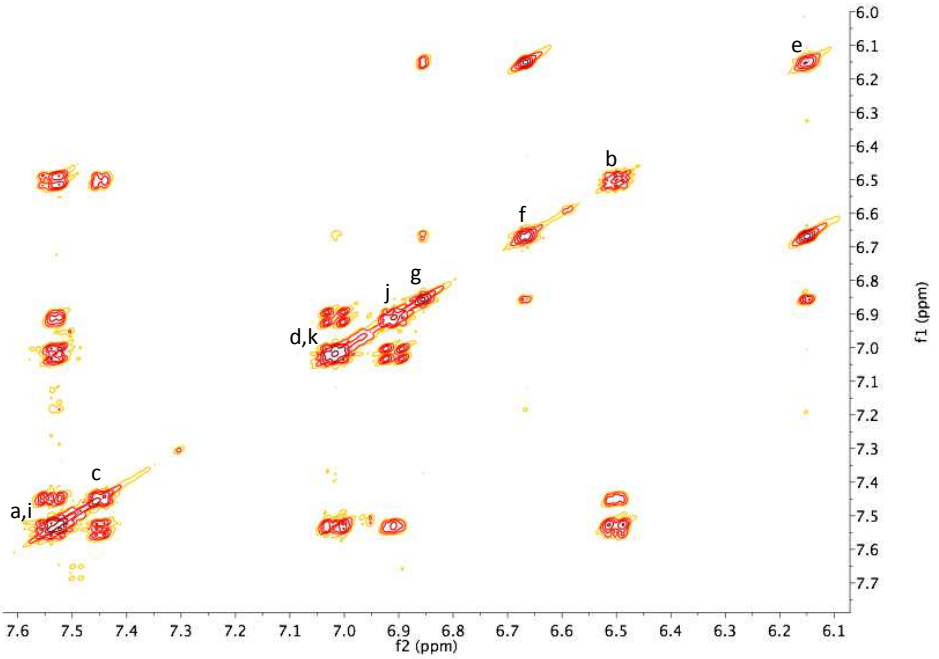

Figure 1.14 COSY spectrum of (pypyr)PtPh(SMe$_2$) in THF-d_8 at 298K.

Synthesis of ^{Me}pypyr–H ligand:

A 50 mL glass reaction flask was charged with palladium acetate (14 mg, 0.062

mmol), 2-dicyclohexylphosphino-2',6'-dimethoxybiphenyl (SPhos) (70 mg, 0.17 mmol), toluene (1 mL) and THF (1 mL). The solvents were removed under vacuum after 10 min to yield a white powder. The reaction vessel was then charged with K_3PO_4 (1.73 g, 8.15 mmol), 2-chloro-6-methylpyridine (0.4 mL, 3.67 mmol), N-Boc-pyrrole-2-boronic acid (700 mg, 3.17 mmol), and *n*-butanol (8 mL) under N_2. The reaction was heated at 100 °C for 48 hours. The crude product was isolated in vacuo, absorbed onto silica gel and purified by column chromatography (1:3 EtOAc:hexanes) R_f = 0.19. Evaporation of the solvent resulted in isolation of white solid of ^{Me}pypyr–H in 42% yield (127 mg, 0.80 mmol). ^{1}H NMR (301 MHz, C_6D_6, 298 K): δ 9.39 (s, br, 1H), 7.07 (d, 1H), 7.01 (t, 1H), 6.72 (m, 1H), 6.49 (d, 1H), 6.44 (m, 1H), 6.33 (m, 1H), 2.37 (s, 3H) ^{13}C{^{1}H} NMR (125 MHz, C_6D_6, 298 K): δ 157.77, 150.83, 136.87, 132.25, 119.91, 119.85, 115.29, 110.67, 107.66, 24.72.

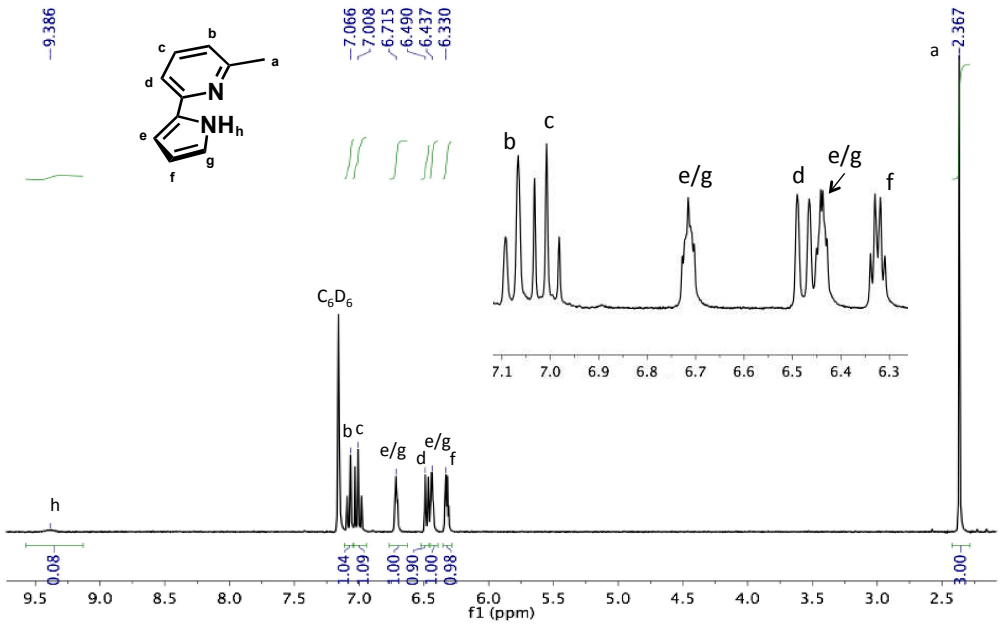

Figure 1.15 ^{1}H NMR spectrum of ^{Me}pypyr–H in C_6D_6 at 298 K.

Synthesis of (^{Me}pypyr)PtPh(SMe_2) (4):

A solution of ^{Me}pypyr–H ligand (23.1 mg, 0.146 mmol) in C_6H_6 was added dropwise to a stirring solution of $[PtMe_2(SMe_2)]_2$ (59.8 mg, 0.073 mmol) in C_6H_6 (3 mL) in a Teflon valve sealable reaction flask. The yellow mixture was stirred for 2 hours at 25 °C. Removal of solvent in vacuo resulted in a dark gold powder/crystalline solid. Recrystallization from toluene/Et_2O resulted in formation of (^{Me}pypyr)PtPh(SMe_2) as a yellow powder in 19% yield (59.8 mg, 0.638 mmol). ^{1}H NMR (700 MHz, C_6D_6, 298 K): δ 7.66 (d, J_{HH} = 7.8 Hz, 2H), 7.11 (t, 2H), 7.07 (t, 2H), 6.90 (dd, 1H), 6.84 (t, 1H), 6.56 (m, 1H), 6.44 (m, 1H), 6.14 (d, 1H), 2.32 (s, 3H), 1.44 (s, $^3J_{PtH}$ = 50.6 Hz, 6H) ^{13}C{^{1}H} NMR (125 MHz, C_6D_6, 298 K): δ 141.74, 138.03, 137.51, 136.76, 133.85, 128.68, 127.72, 123.88, 118.97, 115.37, 111.66, 110.52, 26.68, 21.45. Anal. Calcd. for $C_{18}H_{20}N_2SPt$: C, 43.99; H, 4.10; N, 5.70. Found: C, 43.93; H, 4.02; N, 5.63.

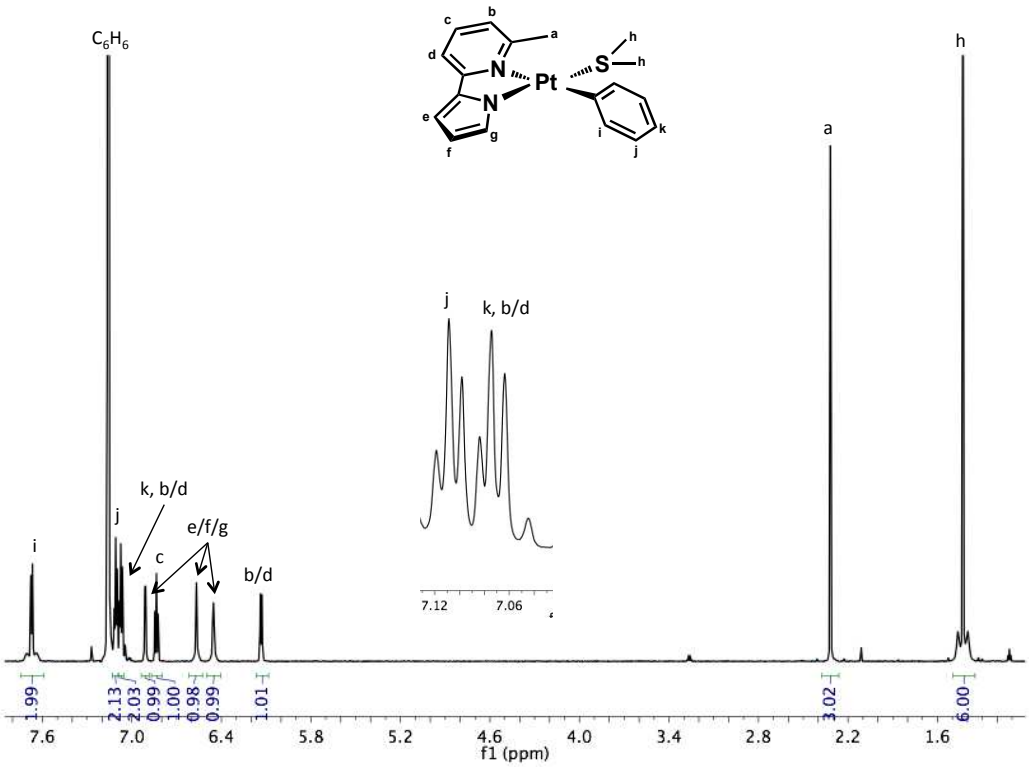

Figure 1.16 ^{1}H NMR spectrum of (^{Me}pypyr)PtPh(SMe$_2$) in C_6D_6 at 298 K.

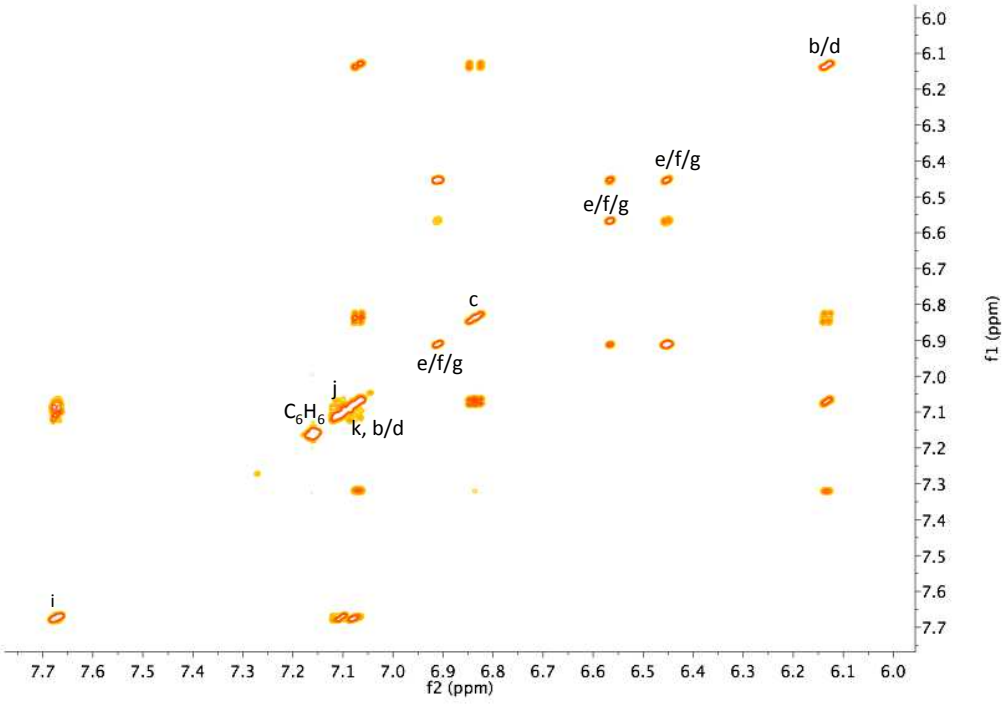

Figure 1.17 COSY spectrum of (^{Me}pypyr)PtPh(SMe$_2$) in C_6D_6 at 298 K.

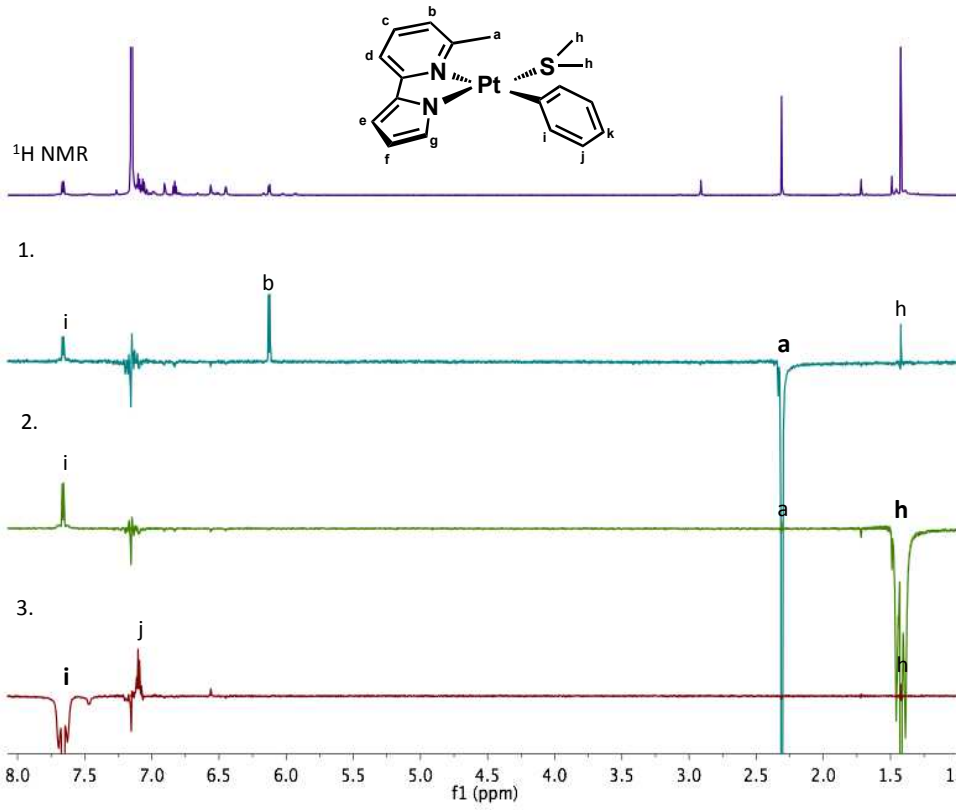

Figure 1.18 1D NOE spectra of (^{Me}pypyr)PtPh(SMe$_2$) in C_6D_6 at 298 K. Top: ^{1}H NMR spectrum used as a background spectrum to subtract all of the non-irradiated peaks in 1, 2, and 3 below. 1. The sample was irradiated at **a** and an NOE enhancement was observed for i, b, h. 2. The sample was irradiated at **h** and an NOE enhancement was observed for i, a. 3. The sample was irradiated at **i** and an NOE enhancement was observed for j and h.

Synthesis of (py-ph-pyr)PtPh(SMe$_2$) (5):

A solution of py-ph-pyr–H (24.6 mg, 0.146 mmol) in C_6H_6 (3 mL) was added dropwise to a stirring solution of [PtPh$_2$(SMe$_2$)]$_2$ (59.8 mg, 0.073 mmol) in C_6H_6 (3 mL) in a Schlenk flask. The mixture was an orange color and was stirred for 3 hours at 25 °C. The solvent was removed in vacuo to yield a yellow solid. Recrystallization in CH_2Cl_2/pentane resulted in (py-ph-pyr)PtPh(SMe$_2$) as a dark yellow powder in 50% yield (36.6 mg, 0.073 mmol). ^{1}H NMR (500 MHz, C_6D_6, 298 K): δ 7.96 (d, 1H),

7.78 (m , 3H), 7.47 (m, 2H), 7.23 (m, 2H), 7.12 (d, 1H), 7.00 (d, 2H), 6.23 (m, 1H), 1.68 (s, $^{3}J_{PtH}$ = 61.3 Hz, 6H)

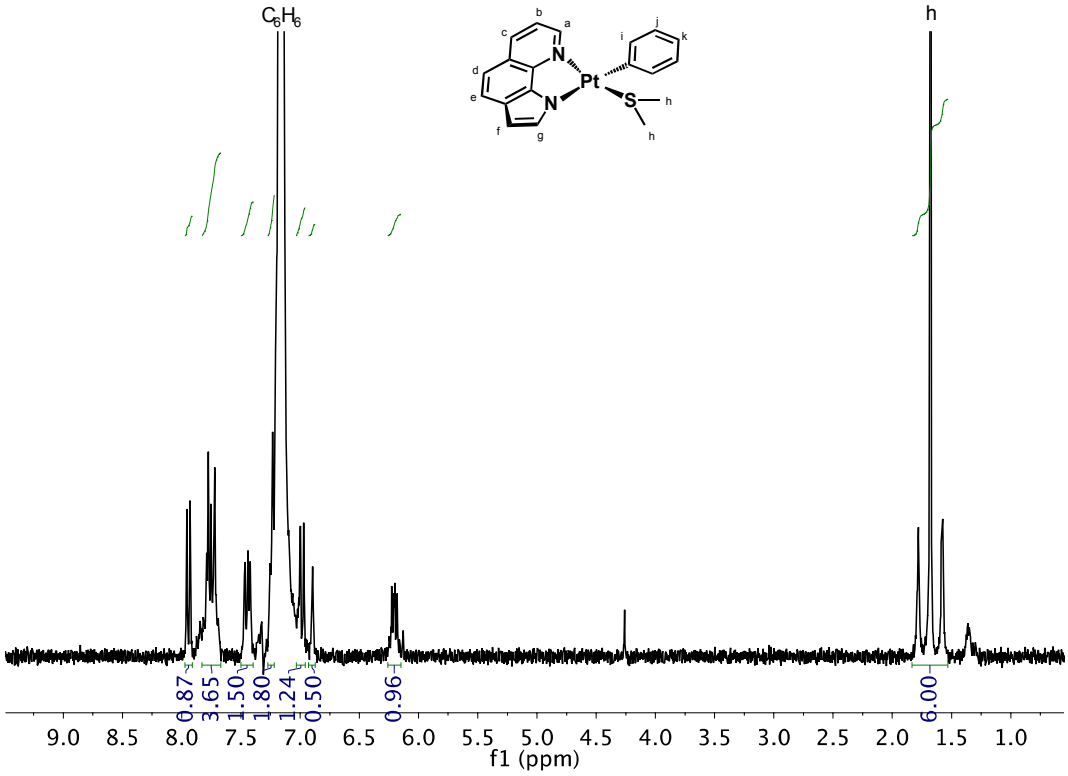

Figure 1.19 ^{1}H NMR spectrum of (py-ph-pyr)PtPh(SMe$_2$) in C_6D_6 at 298 K.

(3,3-dimethylbutyl)-benzene synthesis:

A mixture of *cis* and *trans* β-tert-butylstyrene was synthesized from a Wittig reaction of trimethylacetaldehyde using benzyltriphenylphosphonium bromide and *n*-butyllithium. ^{1}H NMR spectroscopy data is consistent with a previous reported synthesis of β-tert-Butylstyrene.[29] Benzyltriphenyl phosphonium bromide (3 g, 6.9 mmol) and THF (35 mL) was added to a round bottom flask and placed under N_2. The mixture was cooled to –78°C and *n*-BuLi (4.8 mL, 7.6 mmol, 1.6 M) was added

dropwise to the mixture. After one hour of reacting at -78 °C, the mixture was warmed to 0 °C over 10 min. Pivaldehyde (0.75 mL, 6.9 mmol) was added to the reaction and then stirred for 2 hours. Excess *n*-BuLi was quenched by addition of methanol (1.5 mL). The lithium salts were filtered through a medium fritted filter, and the solvent was evaporated off. The product (3,3-dimethylphenylbutene) was purified by flash column chromatography and was isolated as a clear liquid in 24% yield (264 mg, 1.6 mmol). ^{1}H NMR (300 MHz, $CDCl_3$, 298 K): δ 7.18 (m, 5H), 6.37 (d, 1H), 6.26 (d, 1H), 5.57 (d, 1H), 1.11 (s, 9H), 0.97 (s, 9H).

(3,3-dimethyl)butylbenzene was synthesized from a Pd/C hydrogenation of 3,3-dimethylphenylbutene. A Parr Reaction vessel was charged with *cis*- and *trans*-β-tert-Butylstyrene (100 mg, 0.56 mmol), ethanol (1.0 mL), and Pd/C (25 mg, 0.012 mmol Pd^0, 5% w/w). The reaction vessel was sealed and H_2 gas (50 bar) was added to the reaction vessel. The mixture was allowed to react at 25 °C for 24 hours. The product and ethanol was filtered through a FTPE syringe filter, and the ethanol was removed under vacuum. The product was isolated as a clear liquid in 49% yield (44.3 mg, 0.27 mmol). ^{1}H NMR (300 MHz, $CDCl_3$, 298 K): δ 7.21 (m, 5H), 2.56 (m, 2H), 1.49 (m, 2H), 0.95 (s, 9H). ^{1}H NMR spectroscopy data is consistent with a previously reported synthesis of (3,3-dimethyl)butylbenzene.[30]

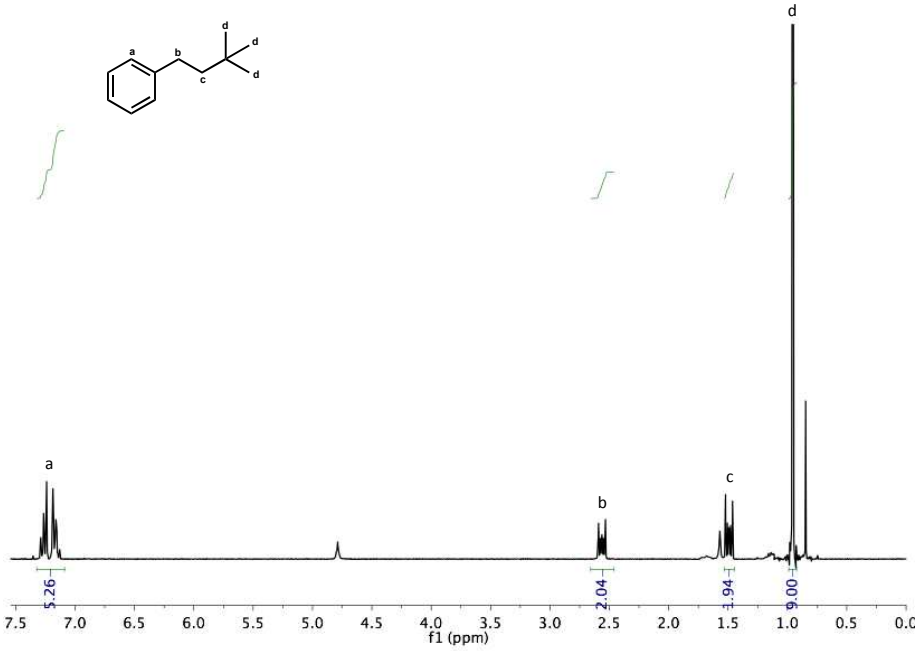

Figure 1.20 ^{1}H NMR spectrum of (3,3-dimethyl)butylbenzene in $CDCl_3$ at 298 K.

3,3-Dimethyl-2-phenyl-butene (α-tert-butyl styrene) synthesis:

A solution of methyltriphenylphosphonium iodide (3.0 g) in THF (55 mL) was added to a flask. This was cooled to −78 °C and placed under N_2. *n*-BuLi (5.1 mL, 1.6 M) was added dropwise to the solution. The reaction turned a light yellow and was allowed to react for 1.5 hours. The reaction was then warmed to 0 °C, and pivalophenone (1.36 mL) was added to the reaction. The reaction was then allowed to react for 2 more hours. Any remaining *n*-BuLi was quenched with methanol and the solvent was removed under vacuum. The crude product was purified by column chromatography (R_f = 0.78, hexanes) to obtain a clear liquid in 59% yield (690 mg, 4.3 mmol). ^{1}H NMR (300 MHz, $CDCl_3$): δ 7.26 (m, 3H), 7.12 (m, 2H), 5.15 (d, 1H), 4.74 (d, 1H), 1.10 (s, 9H).

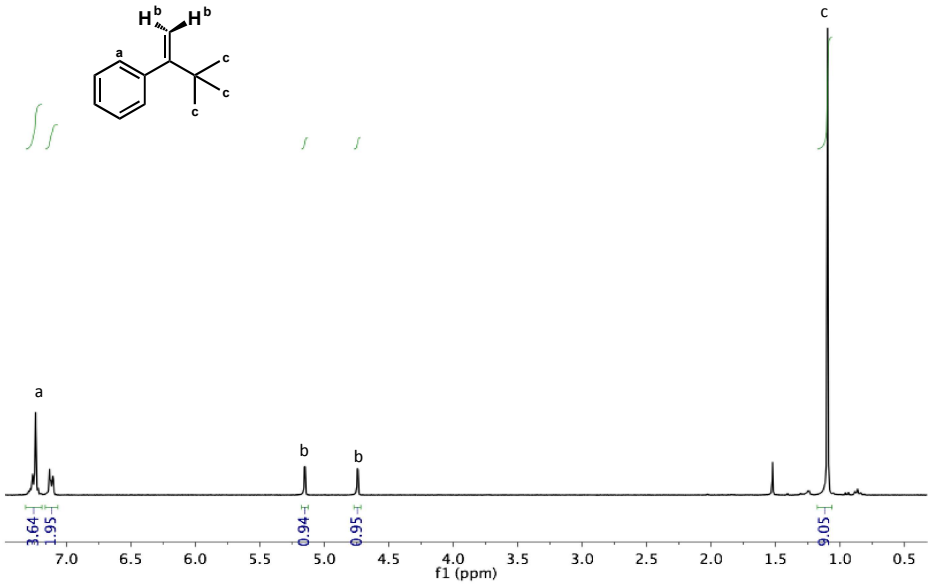

Figure 1.21 ^{1}H NMR spectrum of α -*t*.butylstyrene in $CDCl_3$ at 298 K.

Isomerization studies of (pypyr)PtPh(SMe$_2$) (3) and (^{Me}pypyr)PtPh(SMe$_2$) (4) :

On the bench top, 3.6 mg of the pre-catalyst was weighed and added to a medium-walled J-Young style tube. In the glove box, a solution of hexamethylbenzene (0.0049 mM) in C_6D_6 was prepared. 0.50 mL of the hexamethylbenzene solution was added to each tube. The tubes were sealed and removed from the glove box. The tubes were heated to 100 °C in an oil bath and monitored daily by ^{1}H NMR spectroscopy.

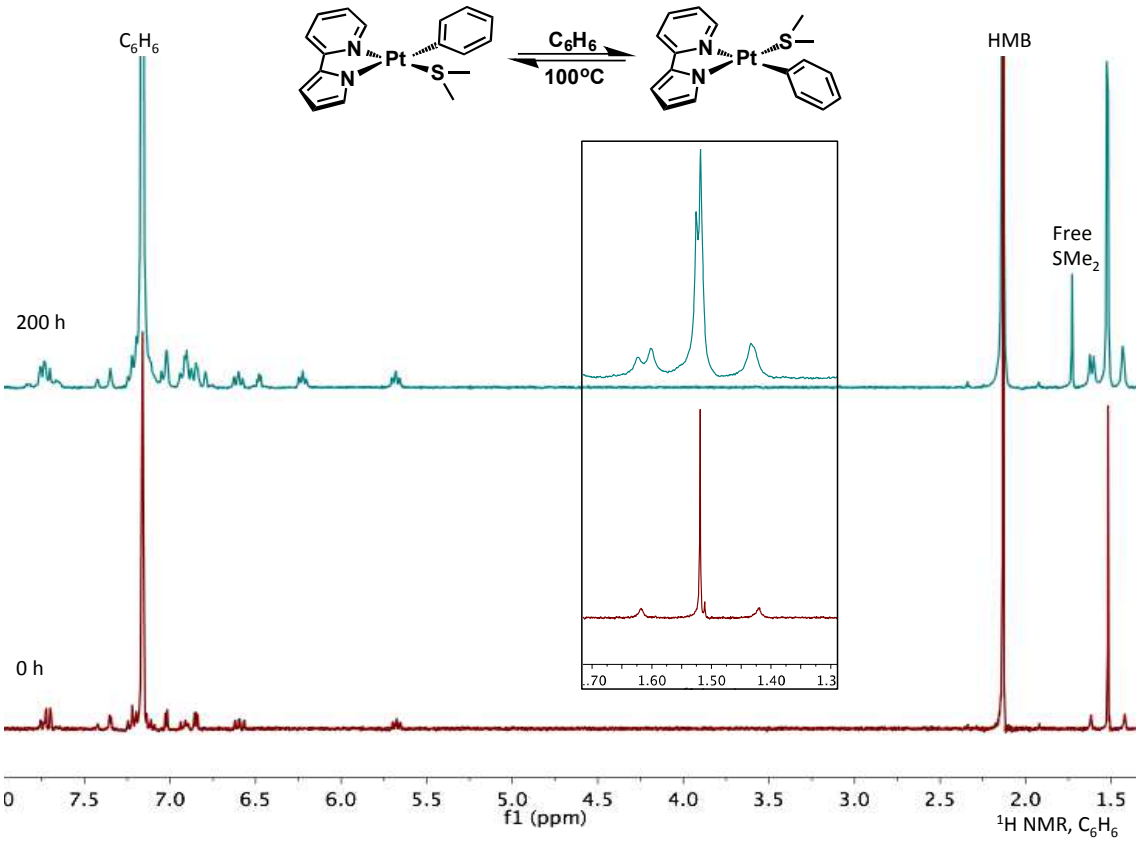

Figure 1.22 ^{1}H NMR spectra (C_6D_6) for thermolysis of (pypyr)PtPh(SMe$_2$) (**3**). Bottom spectrum is before heating and the top is after heating the sample for 200 hours at 100 °C. Inset shows an expansion of the dimethyl sulfide signal for **3** in the bottom spectrum and signals for both isomers in the top spectrum.

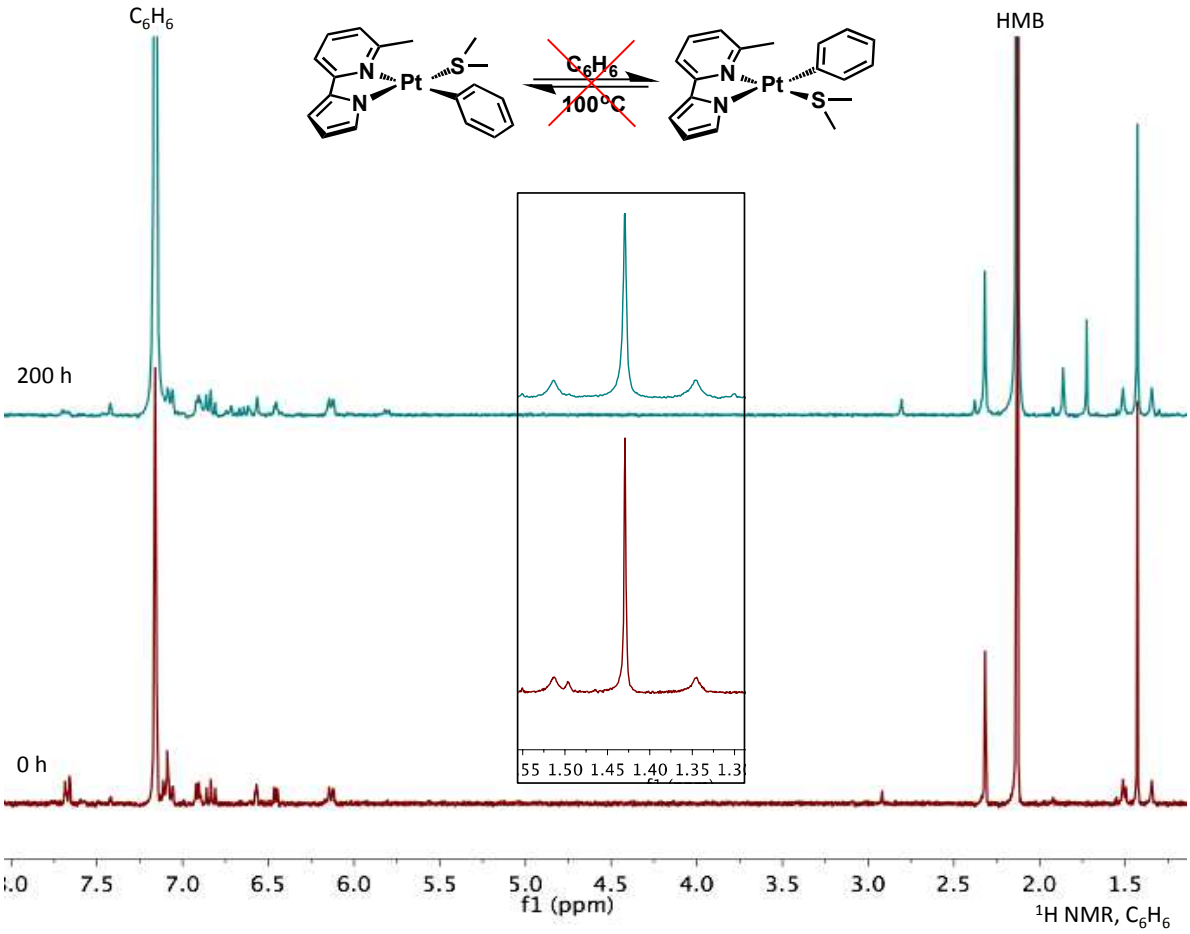

Figure 1.23 ^{1}H NMR spectra (C_6D_6) for of (^{Me}pypyr)PtPh(SMe_2) (**4**). Bottom spectrum is before heating and the top is after heating the sample for 200 hours at 100 °C. Inset shows an expansion of the dimethyl sulfide signal for **4** and no visible signal for a second isomer is evident. However, some decomposition of **4** (34%) was observed after heating and free ligand was identified among the decomposition products.

Hydroarylation reactions:

General procedure for hydroarylation with (pypyr)PtPh(SMe_2):

Stock solutions of (pypyr)PtPh(SMe_2) (0.014 mM) and hexamethylbenzene (0.0049 mM) in benzene were prepared. Using a micro syringe, 0.25 mL of each stock solution was added to three separate medium-walled J-Young style tubes. The tubes were degassed using 3 freeze-pump-thaw cycles on a high vacuum line. The solution was frozen with liquid nitrogen and propylene (11.36 mg, 0.27 mmol, 308 torr) was condensed into each tube using a known volume bulb (16.27 mL). The tubes were sealed and the reaction mixtures heated at 100 °C for 120 hours. Each day the signals for *n*-propylbenzene and cumene were observed by ^{1}H NMR spectroscopy (500 MHz). These signals matched those of the authentic samples.

Hydroarylation results:

Table 2 Hydroarylation TON and ratio of products obtained by GC-FID.[a,b]

Catalyst	Olefin (M)	Product	Product (mmol)	Product Ratios	TON	TOF (hrs^{-1})
1	propylene (0.54)	*n*-propylbenzene	0.0080[c]	12.9	2.2	0.02
		cumene	0.0526	84.1	14.6	0.12
		α-methylstyrene	0.0019	3.0	0.5	0.00
2	(0.54)	*n*-propylbenzene	0.0181	48.3	5.0	0.04
		cumene	0.0193	51.7	5.4	0.04
3	(0.54)	*n*-propylbenzene	0.0184	48.0	5.1	0.04
		cumene	0.0200	52.0	5.5	0.05
	(0.26)	*n*-propylbenzene	0.0159	47.4	4.4	0.04
		cumene	0.0177	52.6	4.9	0.04
	(0.80)	*n*-propylbenzene	0.0275	49.4	7.7	0.06
		cumene	0.0282	50.6	7.8	0.07
4	(0.54)	*n*-propylbenzene	0.0002	1.5	0.1	0.00
		cumene	0.0013	9.8	0.4	0.00

		α-methylstyrene	0.0059	45.0	1.6	0.01
		disubstituted	0.0030	22.9	0.8	0.01
		disubstituted	0.0017	12.8	0.5	0.00
		disubstituted	0.0002	1.9	0.1	0.00
		disubstituted	0.0001	1.1	0.0	0.00
		disubstituted	0.0007	5.1	0.2	0.00
5	(0.54)	*n*-propylbenzene	0.0078	56.7	2.2	0.02
		cumene	0.0060	43.3	1.7	0.01
1	1-hexene (0.51)	hexylbenzene	0.0068	15.9	1.9	0.02
		1-methyl-1pentyl benzene	0.0352	83.1	9.8	0.08
		(1-methylenehexyl)-benzene	0.0004	1.0	0.1	0.00
3	(0.51)	hexylbenzene	0.0173	57.4	4.8	0.04
		1-methyl-1pentyl benzene	0.0129	42.6	3.6	0.03
	(0.51)[d]	hexylbenzene	0.0240	57.0	6.7	0.03
		1-methyl-1pentyl benzene	0.0181	43.0	5.0	0.02
	(0.51)[d,e]	hexylbenzene	0.0351	53.4	9.7	0.04
		1-methyl-1pentyl benzene	0.0288	43.9	8.0	0.03
		(1-methylenehexyl)-benzene	0.0017	2.7	0.5	0.00
	(1.6)	hexylbenzene	0.0188	58.5	5.2	0.04
		1-methyl-1pentyl benzene	0.0134	41.5	3.7	0.03
	(1.6)[d]	hexylbenzene	0.0218	57.5	6.1	0.03
		1-methyl-1pentyl benzene	0.0161	42.5	4.5	0.02
	(2.7)[e]	hexylbenzene	0.0276	59.1	7.7	0.06
		1-methyl-1pentyl benzene	0.0191	40.9	5.3	0.04
	(2.7)[d,e]	hexylbenzene	0.0270	58.6	7.5	0.03
		1-methyl-1pentyl benzene	0.0190	41.4	5.3	0.02
5	(0.51)	hexylbenzene	0.0113	61.5	3.1	0.01
		1-methyl-1pentyl benzene	0.0067	36.3	1.8	0.01
		(1-methylenehexyl)-benzene	0.0004	2.2	0.11	0.00
1	neohexene (0.51)	(3,3-dimethylbutyl)-benzene	0.0094	15.1	0.4	0.00
		(1,2,2-trimethylpropyl)-benzene	0.0005	47.1	1.2	0.01
		α -*t*.butylstyrene	0.0012	37.8	1.0	0.01
3	(0.51)	(3,3-dimethylbutyl)-benzene	0.0014	84.9	2.6	0.02
		(1,2,2-trimethylpropyl)-benzene	0.0043	4.6	0.1	0.00
		α -*t*.butylstyrene	0.0033	10.5	0.3	0.00
	(2.6)	(3,3-dimethylbutyl)-benzene	0.0381	90.0	10.6	0.09
		(1,2,2-trimethylpropyl)-benzene	0.0039	9.3	1.1	0.01
		α -*t*.butylstyrene	0.0003	0.7	0.1	0.00

5	(0.51)	(3,3-dimethylbutyl)-benzene	0.0795	96.0	22.1	0.18
		(1,2,2-trimethylpropyl)-benzene	0.0032	3.9	0.9	0.01
		α -*t*.butylstyrene	0.0001	0.1	0.0	0.00

[a] Experimental conditions: 0.1–1.0 mmol olefin, 1.3 mol% catalyst, excess C6H6, 100 °C, 120 hours. [b] Experiments were conducted 2–3 times and averaged. [c] Standard Deviation [d] Experiment run for 240 hours. [e] Experiment run at 120 °C.

X-ray crystal data:

For all structures below, solution by direct methods (SHELXS, SIR97[31]) produced a complete heavy atom phasing model consistent with the proposed structure. The structure was completed by difference Fourier synthesis with SHELXL97.[32,33] Scattering factors are from Waasmair and Kirfel[34]. Hydrogen atoms were placed in geometrically idealised positions and constrained to ride on their parent atoms with C–H distances in the range 0.95–1.00 Å. Isotropic thermal parameters U_{eq} were fixed such that they were 1.2 U_{eq} of their parent atom U_{eq} for CH's and 1.5 U_{eq} of their parent atom U_{eq} in case of methyl groups. All non-hydrogen atoms were refined anisotropically by full-matrix least-squares.

Precatalyst 1, ($py^{Me2}pyr$)PtPh(SMe_2):

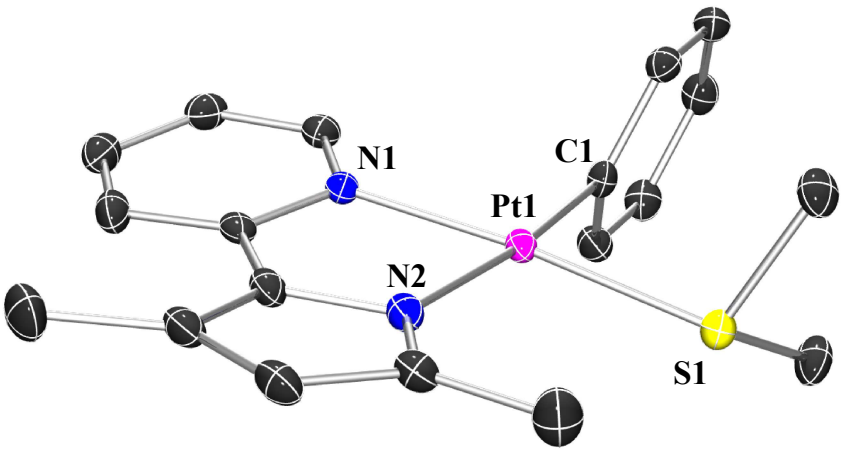

Figure 1.24 POV-Ray diagram of **1** shown with thermal ellipsoids at the 50% probability level. Hydrogen atoms omitted for clarity. Selected bond lengths (Å) and angles (°): C1–Pt1 = 2.0131(17), N1–Pt1 = 2.0538(15), N2–Pt1 = 2.0888(15), S1–Pt1 = 2.2606(6), C1–Pt1–N1 = 93.12(6), C1–Pt1–N2 = 172.74(6), C1–Pt1–S1 = 90.51(5), N1–Pt1–N2 = 79.63(6), N1–Pt1–S1 = 174.99(4), N2–Pt1–S1 = 96.75(4).

Crystals were grown by a diffusion recrystallization. The product was taken up in toluene and filtered through a Teflon syringe filter into a small vial. This was then added to a large vial filled with Et_2O, and capped. X-ray quality crystals were obtained after 7 days of slow solvent diffusion at ambient temperature. Crystal data is given in Table 3.

An orange prism, measuring 0.15 × 0.12 × 0.10 mm^3 was mounted on a loop with oil. Data was collected at –173 °C on a Bruker APEX II single crystal X-ray diffractometer, Mo-radiation.

Crystal-to-detector distance was 40 mm and exposure time was 10 seconds per degree for all sets. The scan width was 0.5°. Data collection was 100% complete to 25° in ϑ. A total of 80242 reflections were collected covering the indices, h = –12 to 12, k = –11 to 11, l = –30 to 30. 4487 reflections were symmetry independent and the R_{int} = 0.0387 indicated that the data was better than average quality (0.07). Indexing and unit cell refinement indicated a primitive monoclinic lattice. The space group was found to be P $2_1/c$ (No.14).

The data was integrated and scaled using SAINT, SADABS within the APEX2 software package by Bruker.[35]

Table 3 Crystallographic data for the structures provided.

Empirical formula	C19 H22 N2 Pt S	
Formula weight	505.54	
Temperature	100(2) K	
Wavelength	0.71073 Å	
Crystal system	Monoclinic	
Space group	P 2_1/c	
Unit cell dimensions	a = 9.309(2) Å	α = 90°.
	b = 8.3834(18) Å	β = 93.843(10)°.
	c = 22.936(5) Å	γ = 90°.
Volume	1785.9(7) Å3	
Z	4	
Density (calculated)	1.880 mg/m^3	
Absorption coefficient	7.974 mm^{-1}	
F(000)	976	
Crystal size	0.15 × 0.12 × 0.10 mm^3	
Theta range for data collection	1.78 to 28.40°.	
Index ranges	–12<=h<=12, –11<=k<=11, –30<=l<=30	
Reflections collected	80242	
Independent reflections	4487 [R(int) = 0.0387]	
Completeness to theta = 25.00°	100.00%	
Max. and min. transmission	0.5027 and 0.3809	
Refinement method	Full-matrix least-squares on F2	
Data / restraints / parameters	4487 / 0 / 210	
Goodness-of-fit on F2	1.112	
Final R indices [I>2sigma(I)]	R1 = 0.0117, wR2 = 0.0261	
R indices (all data)	R1 = 0.0133, wR2 = 0.0267	
Largest diff. peak and hole	0.356 and –0.658 e.$Å^{-3}$	

Precatalyst 3, (pypyr)PtPh(SMe$_2$):

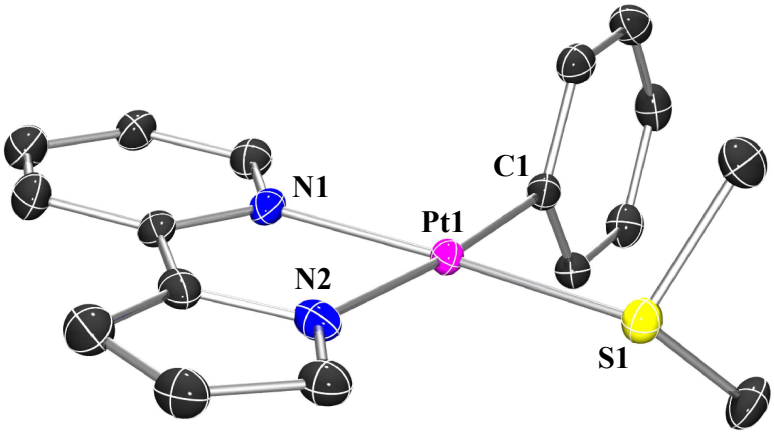

Figure 1.25 POV-Ray diagram of **3** shown with thermal ellipsoids at the 50% probability level. Hydrogen atoms omitted for clarity. Selected bond lengths (Å) and angles (°) for **3**: C1–Pt1 = 2.015(2), N1–Pt1 = 2.047(2), N2–Pt1 = 2.068(2), S1–Pt1 = 2.2490(6), C1–Pt1–N1 = 94.44(9), C1–Pt1–N2 = 173.81(9), C1–Pt1–S1 = 93.32(7), N1–Pt1–N2 = 79.48(8), N1–Pt1–S1 = 172.07(6), N2–Pt1–S1 = 92.72(6).

Crystals were grown by heating the product in THF. The product was taken up in THF in a medium-walled J-Young style tube. This was then freeze-pump-thawed for 3 cycles, and then lightly heated. X-ray quality crystals were obtained after 5 days at ambient temperature. Crystal data is given in Table 4.

A yellow prism, measuring 0.17 × 0.10 × 0.05 mm^3 was mounted on a loop with oil. Data was collected at –173 °C on a Bruker APEX II single crystal X-ray diffractometer, Mo-radiation.

Crystal-to-detector distance was 40 mm and exposure time was 30 seconds per frame for all sets. The scan width was 0.5°. Data collection was 100% complete to 25° in ϑ. A total of 102083 reflections were collected covering the indices, h = –23 to 23, k = –11 to 11, l = –29 to 29. 4044 reflections were symmetry independent and the R_{int} = 0.0312 indicated that the data was brilliant (average quality 0.07).

Indexing and unit cell refinement indicated a primitive orthorhombic lattice. The space group was found to be P b c a (No.61).

The data was integrated and scaled using SAINT, SADABS within the APEX2 software package by Bruker.[35]

Table 4 Crystallographic data for the structures provided.

Empirical formula	C17 H18 N2 Pt S	
Formula weight	477.48	
Temperature	100(2) K	
Wavelength	0.71073 Å	
Crystal system	Orthorhombic	
Space group	P b c a	
Unit cell dimensions	a = 17.162(3) Å	α = 90°.
	b = 8.3320(15) Å	β = 90°.
	c = 21.664(4) Å	γ = 90°.
Volume	3097.9(9) $Å^3$	
Z	8	
Density (calculated)	2.048 mg/m^3	
Absorption coefficient	9.188 mm^{-1}	
F(000)	1824	
Crystal size	0.17 × 0.10 × 0.05 mm^3	
Theta range for data collection	1.88 to 28.80°.	
Index ranges	–23<=h<=23, –11<=k<=11, –29<=l<=29	
Reflections collected	102083	
Independent reflections	4044 [R(int) = 0.0312]	
Completeness to theta = 25.00°	100.00%	
Max. and min. transmission	0.6566 and 0.3042	
Refinement method	Full-matrix least-squares on F2	
Data / restraints / parameters	4044 / 0 / 192	
Goodness-of-fit on F2	1.165	
Final R indices [I>2sigma(I)]	R1 = 0.0151, wR2 = 0.0311	
R indices (all data)	R1 = 0.0208, wR2 = 0.0340	
Largest diff. peak and hole	1.081 and –0.467 $e.Å^{-3}$	

Precatalyst 4, (^{Me}pypyr)PtPh(SMe$_2$):

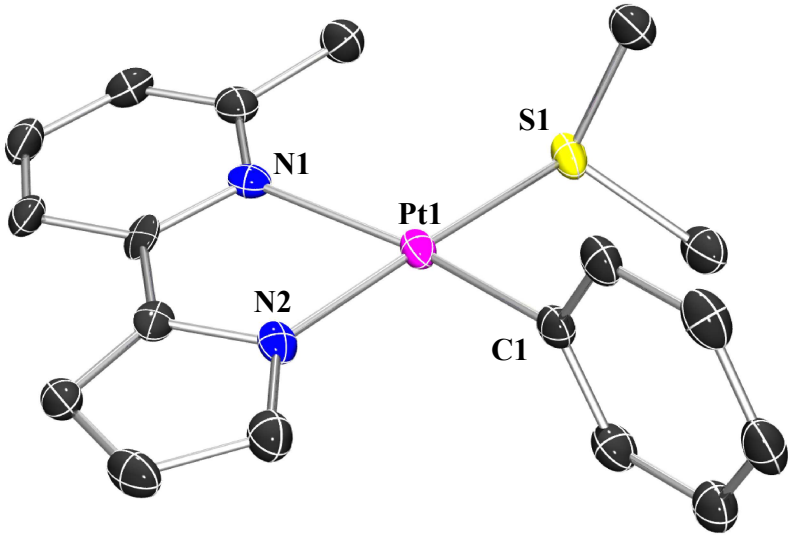

Figure 1.26 POV-Ray diagram of **4** shown with thermal ellipsoids at the 50% probability level. Hydrogen atoms omitted for clarity. Selected bond lengths (Å) and angles (°) for 4: C1–Pt1 = 1.994(5), N1–Pt1 = 2.220(4), N2–Pt1 = 2.002(4), S1–Pt1 = 2.2736(13), C1–Pt1–N1 = 168.98(17), C1–Pt1–N2 = 90.47(18), C1–Pt1–S1 = 89.37(14), N1–Pt1–N2 = 78.81(16), N1–Pt1–S1 = 101.44(11), N2–Pt1–S1 = 177.76(12).

Crystals were grown by a diffusion recrystallization. The product was taken up in toluene and filtered through a Teflon syringe filter into a small vial. This was then added to a large vial filled with Et_2O, and capped. X-ray quality crystals were obtained after 7 days of slow solvent diffusion at –30 °C. Crystal data is given in Table 5.

A yellow plate measuring 0.20 × 0.10 × 0.01 mm^3 which was mounted on a loop with oil. Data was collected at –173 °C on a Bruker APEX II single crystal X-ray diffractometer, Mo-radiation. Crystal-to-detector distance was 40 mm and exposure time was 10 seconds per degree for all sets. The scan width was 0.5°. Data collection was 100% complete to 25° in ϑ.

The raw data appeared twinned. With CELL_NOW[36] a 180° twin operation about (1 0 -1) was found which, if unresolved, would cause considerable overlap of diffraction peak intensities from different domains of the sample. Multi-domain integration with SAINT within the APEX2 software package by Bruker[35] and absorption correction with TWINABS[37] removed the overlap. A total of 7682 (merged) reflections in the HKLF 5 format were collected with 4002 symmetry independent reflections covering the indices, h = –12 to 12, k = –11 to 11, l = 0 to 26 with R_{int} = 0.0538 indicating that the twin-refined data was good (average quality 0.07). Indexing and unit cell refinement indicated then a primitive monoclinic lattice. The space group was found to be P 2_1/n (No.14).

The data was integrated and scaled using SAINT, SADABS within the APEX2 software package by Bruker.[35]

Table 5 Crystallographic data for the structures provided.

Empirical formula	C18 H20 N2 Pt S	
Formula weight	491.51	
Temperature	100(2) K	
Wavelength	0.71073 Å	
Crystal system	Monoclinic	
Space group	P 2_1/n	
Unit cell dimensions	a = 9.4543(11) Å	α = 90°.
	b = 8.8672(10) Å	β = 100.551(6)°.
	c = 20.010(2) Å	γ = 90°.
Volume	1649.1(3) $Å^3$	
Z	4	
Density (calculated)	1.980 mg/m^3	
Absorption coefficient	8.633 mm^{-1}	
F(000)	944	
Crystal size	0.20 × 0.10 × 0.01 mm^3	
Theta range for data collection	2.07 to 28.08°.	
Index ranges	–12<=h<=12, –11<=k<=11, 0<=l<=26	
Reflections collected	131864	
Independent reflections	4002 [R(int) = 0.0538]	
Completeness to theta = 25.00°	100.00%	
Max. and min. transmission	0.9186 and 0.2771	
Refinement method	Full-matrix least-squares on F2	
Data / restraints / parameters	7682 / 0 / 203	
Goodness-of-fit on F2	1.069	
Final R indices [I>2sigma(I)]	R1 = 0.0375, wR2 = 0.0850	
R indices (all data)	R1 = 0.0467, wR2 = 0.0897	
Largest diff. peak and hole	1.613 and –1.106 $e.Å^{-3}$	

Precatalyst 5, (py-ph-pyr)PtPh(SMe_2):

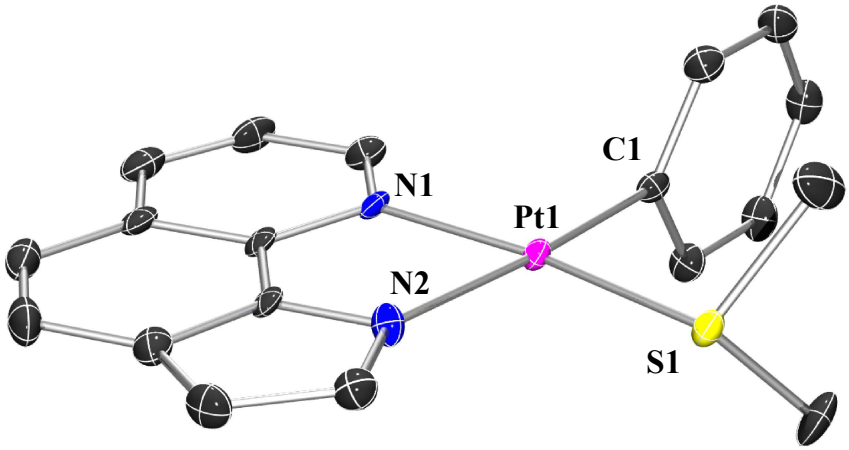

Figure 1.27 POV-Ray diagram of **5** shown with thermal ellipsoids at the 50% probability level. Hydrogen atoms omitted for clarity. Selected bond lengths (Å) and angles (°) for **5**: C1–Pt1 = 2.002(5), N1–Pt1 = 2.079(4), N2–Pt1 = 2.113(4), S1–Pt1 = 2.2443(12), C1–Pt1–N1 = 92.82(17), C1–Pt1–N2 = 174.56(17), C1–Pt1–S1 = 93.79(13), N1–Pt1–N2 = 81.75(15), N1–Pt1–S1 = 173.09(12), N2–Pt1–S1 = 91.65(12).

Crystals were grown by a diffusion recrystallization. The product was taken up in methylene chloride and filtered through a Teflon syringe filter into a small vial. This was then added to a large vial filled with pentane, and capped. X-ray quality crystals were obtained after 7 days of slow solvent diffusion at –30 °C. Crystal data is given in Table 6.

An orange prism, measuring 0.45 x 0.33 x 0.18 mm^3 was mounted on a loop with oil. Data was collected at -173°C on a Bruker APEX II single crystal X-ray diffractometer, Mo-radiation. Crystal-to-detector distance was 40.00 mm and exposure time was 3 seconds per frame for all sets. The scan width was 0.5°. Data collection was 99.6% complete to 25° in ϑ. A total of 50031 reflections were collected covering the indices, h = –14 to 14, k = –20 to 21, l = –11 to 11. 4053 reflections were symmetry independent and the R_{int} = 0.0421 indicated that the data was of greater than average quality (0.07). Indexing and unit cell refinement

indicated a Monoclinic lattice. The space group was found to be P 1 21/c 1 (No.14). The data was integrated and scaled using SAINT, SADABS within the APEX2 software package by Bruker.[35]

Solution by direct methods (SHELXS, SIR97[31]) produced a complete heavy atom phasing model consistent with the proposed structure. The structure was completed by difference Fourier synthesis with SHELXL97.[32,33] Scattering factors are from Waasmair and Kirfel.[34] Hydrogen atoms were placed in geometrically idealised positions and constrained to ride on their parent atoms with C---H distances in the range 0.95-1.00 Angstrom. Isotropic thermal parameters U_{eq} were fixed such that they were 1.2 U_{eq} of their parent atom Ueq for CH's and 1.5 U_{eq} of their parent atom U_{eq} in case of methyl groups. All non-hydrogen atoms were refined anisotropically by full-matrix least-squares.

Table 6 Crystallographic data for the structures provided.

Empirical formula	C19 H18 N2 Pt S	
Formula weight	501.5	
Temperature	95(2) K	
Wavelength	0.71073 Å	
Crystal system	Monoclinic	
Space group	P 2_1/c	
Unit cell dimensions	a = 11.0843(8) Å	α = 90°.
	b = 16.7889(12) Å	β = 98.801(4)°.
	c = 8.7965(7) Å	γ = 90°.
Volume	1617.7(2) Å3	
Z	4	
Density (calculated)	2.059 Mg/m3	
Absorption coefficient	8.803 mm-1	
F(000)	960	
Crystal size	0.45 x 0.33 x 0.18 mm3	
Theta range for data collection	2.22 to 28.66°.	
Index ranges	-14<=h<=14, -20<=k<=21, -11<=l<=11	
Reflections collected	50031	
Independent reflections	4053 [R(int) = 0.0421]	
Completeness to theta = 25.00°	99.60%	
Max. and min. transmission	0.3002 and 0.1097	
Refinement method	Full-matrix least-squares on F2	
Data / restraints / parameters	4053 / 0 / 208	
Goodness-of-fit on F2	1.103	
Final R indices [I>2sigma(I)]	R1 = 0.0340, wR2 = 0.0910	
R indices (all data)	R1 = 0.0375, wR2 = 0.0940	
Largest diff. peak and hole	4.409 and -4.078 e.Å-3	

[1] a) B. V. Vora, G. A. Peterson, S. W. Sohn, M. G. Riley Handbook of Detergents Part F: Detergent Alkylate and Detergent Olefins Production; (Eds: U. Zoller, P. Sosis), CRC Press: New York, N.Y., **2009**.; b) T. Matsumoto , *Catal. Surv. Asia* **2007**, *11*, 31.; c) J. R. Andretta, *J. Organomet. Chem.* **2011**, *696*, 305.

[2] I. Adami Handbook of Detergents Part F: Production of Linear Alkylbenzene Sulfonate and α-Olefin Sulfonates; (Eds: U. Zoller, P. Sosis), CRC Press: New York, N.Y., **2009**.

[3] a) T. Matsumoto, D. J. Taube, R. A. Periana, H. Taube, H. Yo-shida, *J. Am. Chem. Soc.* **2000**, *122*, 7414. b) R. A. Periana, X. Y. Liu, G. Bhalla, *Chem. Commun.* **2002**, *0*, 3000. c) J. Oxgaard, R. P. Muller, W. A. Goddard, R. A. Periana, *J. Am. Chem. Soc.* **2004**, *126*, 352. d) J. Oxgaard, R. A. Periana, W. A. Goddard, *J. Am. Chem. Soc.* **2004**, *126*, 11658. e) G. Bhalla, S. M. Bischof, S. K. Ganesh, X. Y. Liu, C. J. Jones, A. Borzenko, W. J. Tenn, D.

H. Ess, B. G. Hashiguchi, K. S. Lo-kare, C. H. Leung, J. Oxgaard, W. A. Goddard, R. A. Periana, *Green Chem.*, **2011**, *13*, 69.
[4] a) M. Lail, C. M. Bell, D. Conner, T. R. Cundari, T. B. Gunnoe, J. L. Peterson, *Organometallics* **2004**, *23*, 5007. b) N. A. Foley, M. Lail, T. B. Gunnoe, T. R. Cundari, P. D. Boyle, J. L. Petersen *Organometallics* **2007,** *26,* 5507. c) N. A. Foley, M. Lail, J. P. Lee, T. B. Gunnoe, T. R. Cundari, J. L. Petersen *J. Am. Chem. Soc.* **2007**, 129, 6765. d) N. A. Foley, Z. Ke, T. B. Gunnoe, T. R. Cundari, J. L. Petersen *Organometallics* **2008,** *27,* 3007. e) N. A. Foley, M. Lail, T. B. Gunnoe, T. R. Cundari, P. D. Boyle, J. L. Petersen *Organometallics* **2007,** *26,* 5507. f) N. A. Foley, J. P. Lee, Z. Ke, T. B. Gunnoe, T. R. Cundari, *Acc. Chem. Res.* **2009**, *45*, 585. g) E. E. Joslin, C. L. McMullin, T. B. Gunnoe, T. R. Cundari, M. Sabat, W. H. Myers *Organometallics* **2012**, *31*, 6851
[5] B. A. McKeown, N. A. Foley, J. P. Lee, T. B. Gunnoe, *Organometallics* **2008**, *27*, 4031.
[6] B. A. McKeown, B. M. Prince, Z. Ramiro, T. B. Gunnoe, T. R. Cundari, *ACS Catal.* **2014**, 4, 1607.
[7] B. A. McKeown, H. E. Gonzalez, T. Michaelos, T. B. Gunnoe, T. R. Cundari, R. H. Crabtree, M. Sabat, *Organometallics* **2013**, *32*, 3903.
[8] Luedtke, A. T.; Goldberg, K. I. *Angew. Chem. Int. Ed.* **2008**, *47*, 7694.
[9] Clement, M. L.; Grice, K. A.; Luedtke, A. T.; Kaminsky, W.; Goldberg, K. I. *Chem. Eur. J.* 2014, *20*, 17287.
[10] See the Supporting Information
[11] C.H. Langford, H.B. Gray Ligand substitution processes, W.A. Benjamin, 1965.
[12] M.Y. Darensbourg Inorganic Synthesis; John Wiley & Sons Inc.: New York, 1998; Vol. 32.
[13] Rashidi, M.; Fakhroeian, Z.; Puddephatt, R. J. *J. Organomet. Chem.* **1991**, *406*, 261.
[14] Siu, J.; Baxendale, I. R.; Ley, S. V. *Org. Biomol. Chem.*, **2004**, *2*, 160.
[15] Rashidi, M.; Fakhroeian, Z.; Puddephatt, R. J. *J. Organomet. Chem.* **1991**, *406*, 261.
[16] When complex **4** was used the concentrations of products **A** and **B** were quite small and quantification over time by ^{1}H NMR spectroscopy was not viable.
[17] B. A. McKeown, H. E. Gonzalez, T. B. Gunnoe, Cundari, T. R.; Sabat, M. *ACS Catal.* **2013**, *3*, 1165.
[18] B. A. McKeown, H. E. Gonzales, M. R. Friedfeld, T. B. Gunnoe, T. R. Cundari, M. Sabat, *J. Am. Chem. Soc.* **2011**, *133*, 19131.
[19] a) M. A. Bowring, R. G. Bergman, T. D. Tilley, *Organometallics* **2013**, 32, 5266. b) M. A. Bowring, R. G. Bergman, T. D. Tilley, *J. Am. Chem. Soc.* **2013**, 135, 13121
[20] M. Lersch, M. Tilset, *Chem. Rev.* **2005**, *105*, 2471.
[21] Bair, J. S.; Schramm, Y.; Sergeey, A. G.; Clot, E.; Eisenstein, O.; Hartwig, J. F. *J. Am. Chem. Soc.* **2014**, *136*, 13098-13101.
[22] Bauer, J.; Braunschweig, H.; Brenner, P.; Kraft, K.; Radacki, K.; Schwab, K. *Chem. Eur. J.* **2010**, *16*, 11985 – 11992.
[23] Klappa, J. J.; Rich, A. E.; McNeill, K. *Org. Lett.* **2002**, *4*, 435.
[24] Luedtke, A. T.; Goldberg, K. I. *Angew. Chem. Int. Ed.* **2008**, *47*, 7694.
[25] Kudo, N.; Perseghini, M.; Fu, G.C.; *Angew. Chem. Int. Ed.* **2006**, *45*, 1282.
[26] Darensbourg, M. Y. *Inorg. Synth.*; John Wiley & Sons: New York, 1998; Vol. 32, pp 150.
[27] Rashidi, M.; Fakhroeian, Z.; Puddephatt, R. J. *J. Organomet. Chem.* **1991**, *406*, 261.
[28] Siu, J.; Baxendale, I. R.; Ley, S. V. *Org. Biomol. Chem.*, **2004**, *2*, 160.
[29] Dong, D.J.; Li, H.H.; Tian, S.K. *J. Am. Chem. Soc.* **2010**, *132*, 5018.
[30] Antoniolettia, R.; Bonadiesb, F.; Ciammaichellab, A.; Vigliantia, A. *Tetrahedron* **2008**, *64*, 4644.
[31] (a) Altomare, A.; Burla, C.; Camalli, M.; Cascarano, G.L.; Giacovazzo, C.; Guagliardi, A.; Moliterni, A.,G.,G.; Polidori, G.; Spagna, R. *J. Appl. Cryst.*, **1999**, *32*, 115. (b) Altomare, A; Cascarano, G.,L.; Giacovazzo, C.; Guagliardi, A. *J. Appl. Cryst.* **1993**, *26*, 343.

[32] Sheldrick, G. M. SHELXL-97: Program for the Refinement of Crystal Structures 1997 University of Göttingen, Germany.

[33] Mackay, S.; Edwards, C.; Henderson, A.; Gilmore, C.; Stewart, N.; Shankland, K.; Donald, A.; *MaXus: a computer program for the solution and refinement of crystal structures from diffraction data*. University of Glasgow, Scotland, 1997.

[34] Waasmaier, D.; Kirfel, A. *Acta Crystallogr. A.* **1995**, *51*, 416.

[35] Bruker (**2007**) APEX2 (Version 2.1-4), SAINT (version 7.34A), SADABS (version 2007/4), BrukerAXS Inc, Madison, Wisconsin, USA.

[36] Sheldrick, G. M. (2005). CELL_NOW. University of Goettingen, Germany.

[37] Sheldrick, G. M. (2007). TWINABS. University of Goettingen, Germany.

2.0 Tandem catalytic ester hydrogenation and deoxygenation of polyethylene terephthalate:

World consumption of polyethylene terephthalate (PET) is 26 million tons per year.[38] This is mostly for the synthesis of polyester fibers, films, such as Mylar, and plastic drinking bottles. The traditional synthetic route for obtaining PET is a condensation reaction between terephthalic acid and ethylene glycol, Figure 2.1.[39] While PET is a widely utilized plastic, there is growing concern about the environmental impacts of the accumulation and fragmentation of plastics into the environment.[40] This is mainly because food and medical-grade PET cannot be re-incorporated into new resin. Solutions to this problem have focused on two main areas: 1) Utilizing bio-renewable feedstocks as an alternative to a dwindling petroleum supply, and 2) Decreasing the amount of plastics that go into landfills. The problem with the former is that it does not solve the problem of an already enormous amount of PET that is wasted every year after it has been consumed.

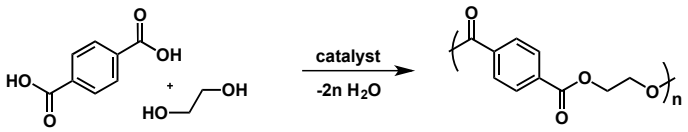

Figure 2.1 Traditional synthesis route of PET

There are many recycling techniques for PET, however these have limitations. Physical reforming and remolding often produces inferior grade PET with shorter chain lengths that can no longer be used for food or medical grade applications. Chemical trans-esterification converts a long chained polymer into short-chained oligomers that can be melt-filtered at low temperatures, but requires high temperatures and pressures. The oligomers can then be fed back into the

production process for polymerization. This method is becoming decreasingly useful as industrial methods for producing PET shift more towards the use of terephthalic acid as the monomer precursor instead of the corresponding methyl ester.[38] This means there is room for improvement in chemical recycling as the current methods prove to be inefficient, and often produce inferior polymer. Thus PET recycling is still not as cost effective as synthesizing PET from virgin resin.

We propose an alternative to current PET recycling methods by the use of a tandem homogeneous catalytic system in which PET is converted to *para*-xylene as shown in Figure 2.2. In the first step of the proposed tandem catalytic cycle, an ester hydrogenation catalyst will be used to hydrogenate PET to ethylene glycol (EG) and 1,4-benzene dimethanol (BDM). In the second step BDM will then be deoxygenated to *p*-xylene with a deoxygenation catalyst. *p*-Xylene could easily be separated from the product mixture via distillation (b.p. = 138.4°C) whereas 1,4-benzenedimethanol separation is much more difficult (b.p. = 138°C/1 mm Hg). Converting used PET back to *p*-xylene will eliminate the generation of oligomers that will produce inferior quality PET. *p*-Xylene can then be fed directly into the current commercial terephthalic acid process and used to produce "virgin" recycled PET. Ultimately, this project was designed to enable recycled PET to be used in a broader range of applications. It was hoped that shared experimental conditions could be found for both catalysts so they would operate in the same system, or that a single catalyst could be found that would be able to perform both transformations.

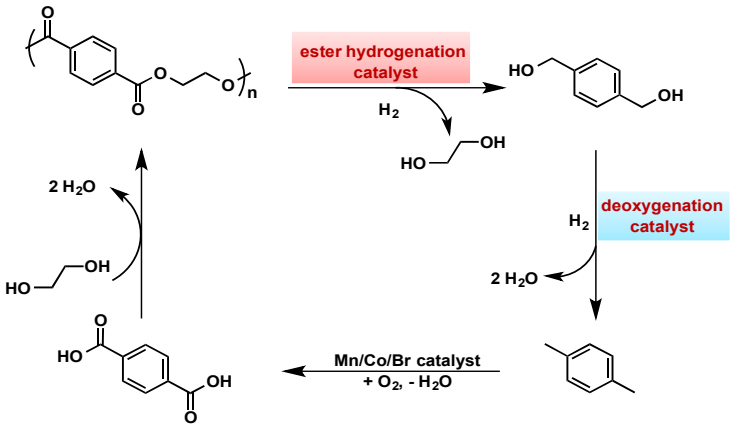

Figure 2.2 Proposed PET cycle

Recently, a Ru(PNN) complex developed by Milstein and coworkers was found to be effective for the dehydrogenative coupling of alcohols to give esters.[41] Robertson and coworkers have demonstrated that the same dearomatized pyridine-based PNN Ru complex, or Ru(PNN)[41], can be used in conjunction with 2 eq. of KO*t*Bu (relative to pre-catalyst to generate the active catalytic species) to obtain BDM and EG as products, Figure 2.3.[42] Moderate temperatures (160 °C) and pressures of H_2 (54.4 atm) were required to effect these transformations.

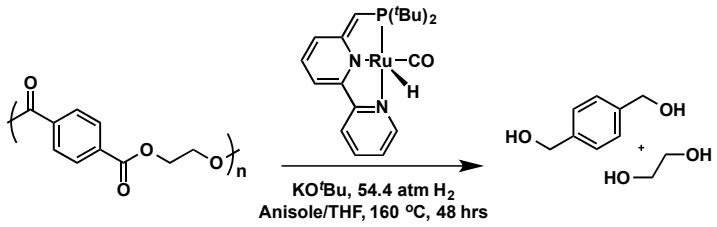

Figure 2.3 Catalytic depolymerization of PET with Milstein's Ru(PNN) complex.

While Robertson's work shows the feasibility of a polyester hydrogenation pathway, a base activated catalyst was employed in the reaction. Catalysts for deoxygenaton of the diol operate under acidic conditions. This would lead to incompatibility of catalysts for a system that would both depolymerize the PET and then deoxygenate the alcohol products.

2.1 Ester Hydrogenation:

Initially, the catalyst Ir(POCOP)^{iPr4}H(CO)Cl (**1**) was chosen for this part of the project as there is precedent for using this type of catalyst for hydrogenation processes under acidic conditions.[43] Ethyl benzoate was chosen as a model substrate as it is structurally similar to 1 PET monomer unit, Figure 2.4. Preliminary testing with **1** to determine if hydrogenation to the corresponding alcohols is possible with an acid tolerant Ir(POCOP) precatalyst, resulted in a 24 and 13% yield to ethanol and benzyl alcohol, respectively by ^{1}H and ^{13}C NMR spectroscopy, Figure 2.5. This result demonstrated the possibility of PET hydrogenation with an Ir(POCOP) catalyst. It is important to note that a higher % yield for ethanol could imply that acid catalyzed ester hydrolysis is contributing to the amount of ethanol generated in the reaction. Benzoic acid, the other product of acid catalyzed hydrolysis, was not observed as a product in the reaction by either ^{1}H or ^{13}C NMR spectroscopy.*

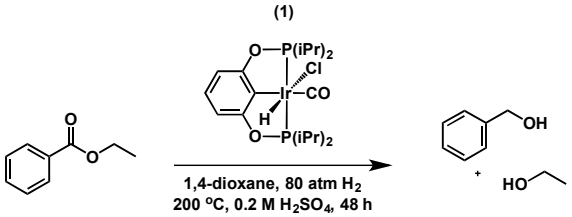

Figure 2.4 Hydrogenation of ethyl benzoate.

* We would expect to see benzoic acid as it is soluble in a water/1,4-dioxane mixture based on these findings J. Chem. Eng. Data 2007, 52, 298 – 300.

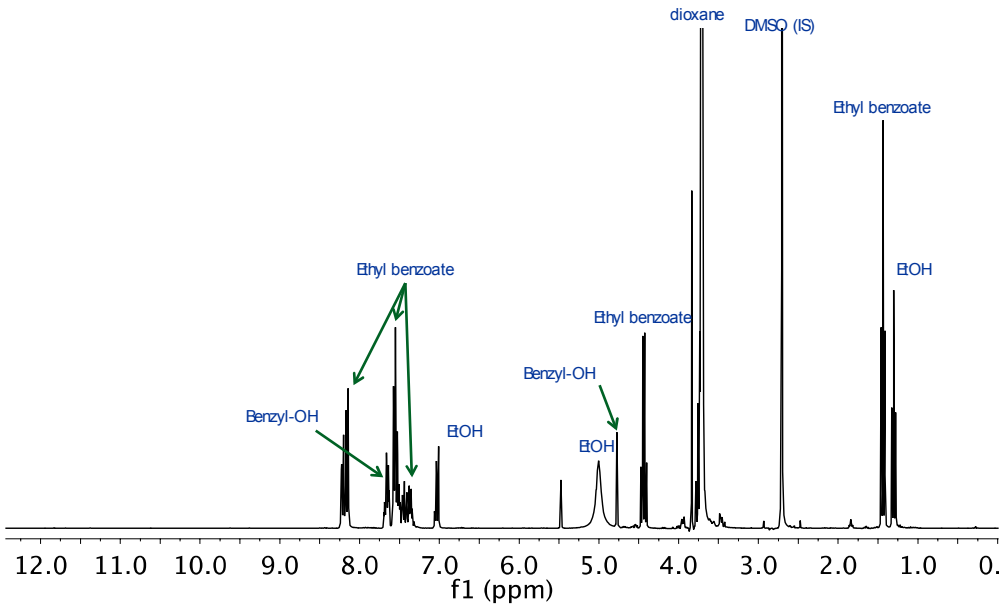

Figure 2.5 ^{1}H NMR spectrum of ethyl benzoate hydrogenation with **1**.

A catalytic cycle is proposed for the hydrogenation of PET with an Ir(POCOP) catalyst in which the activated catalyst, a dihydrogen complex, can act as a proton donor, Figure 2.6. This mechanism is similar to the proposed hydrogenation of carboxylic acids by a half-sandwich iridium catalyst.[44] In step one of the mechanism, the ester is protonated by a dihydrogen hydride iridium intermediate. In the second step, a hydride is transferred to the protonated ester to form a hemiacetal and regenerate the dihydrogen complex with the addition of H_2. The hemiacetal can then decompose to form 1 equivalent of alcohol and aldehyde. The resulting aldehyde can undergo the same mechanism as the ester to generate the corresponding alcohol.

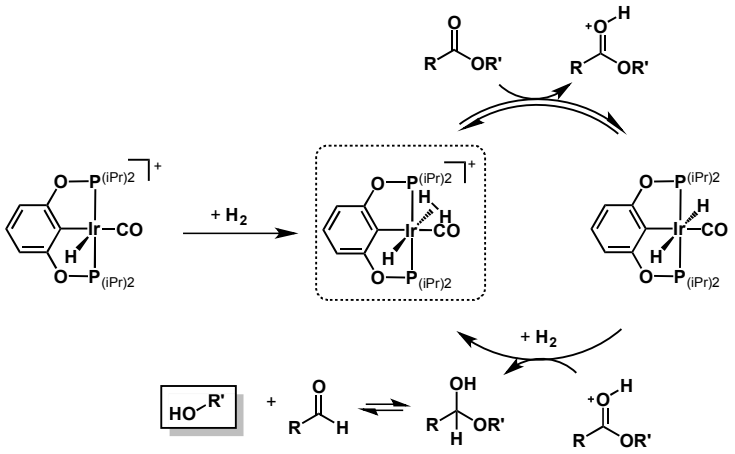

Figure 2.6 Proposed catalytic cycle for the hydrogenation and deoxygenation of PET

2.2 PET hydrogenation with 1:

Hydrogenation of PET with **1** was trialed under similar conditions as used for ethyl benzoate. While EG was observed as a product in these reactions, there was no evidence of BDM in the ^{13}C NMR spectrum (Table 2). ^{13}C NMR signals due to unidentified products, however, were observed in the reactions conducted with PET. It is possible that terephthalic acid could have been generated as the product of acid catalyzed hydrolysis. It would not be observed by either ^{13}C NMR spectroscopy or GC-MS because of the low solubility of terephthalic acid in 1,4-dioxane.

Initially the conditions used for ethyl benzoate were tried but only EG and unidentifiable products were observed. The catalyst loading was increased (entries 1 & 2), and anisole was added to the reaction to help improve the solubility of PET as the solubility in 1,4-dioxane is very low (entry 3). The reaction time was also extended out to see if it was complete after 48 hours, (entry 4). Then the H_2 pressure was altered between 40-80 atm, (entries 5-7), but this did not help

generate BDM. Finally, the temperature was varied between 160-260 °C, but an increase in the TON and % yield was not observed.

Table 2. PET hydrogenation results with **1.**

entry	$p(H_2)$/ atm	substrate (mmol)	catalyst (mmol)	base/acid additive (mmol)	TON (EG:BDM)	% Yield (EG:BDM)
1[a]	80	5.20	0.006	0.05	95.4 : 0.0	11.9 : 0.0
2[a]	80	5.20	0.01	0.05	108.4 : 0.0	13.5 : 0.0
3	80	1.60	0.01	0.05	26.0 : 0.0	21.1 : 0.0
4[b]	80	1.60	0.01	0.05	26.0 : 0.0	21.1 : 0.0
5	40	1.60	0.01	0.05	----	----
6	65	1.60	0.01	0.05	19.5 : 0.0	15.8 : 0.0
7	80	1.60	0.01	0.05	15.2 : 0.0	12.3 : 0.0
8[c]	80	1.60	0.01	0.05	----	----
9[d]	80	1.60	0.01	0.05	15.2 : 0.0	12.3 : 0.0
10[e]	80	1.60	0.01	0.05	23.8 : 0.0	19.4 : 0.0
11[f]	80	1.60	0.01	0.05	----	----

[a] Anisole was not added to the reaction. [b] Reaction time extended out to 120h. [c] 160 °C [d] 220 °C [e] 240 °C [f] 260 °C.

2.3 PET hydrogenation with reported ester hydrogenation catalysts:

Several known complexes capable of ester hydrogenation were also screened for PET hydrogenation, Figure 2.7. The TON and % yield of EG and BDM were determined by quantitative ^{13}C NMR spectroscopy, Figure 2.9. Notably, **5-8** operate under basic conditions, which could be problematic in the proposed reaction cascade due to incompatibility with acidic conditions under which the catalyst Ir(POCOP) operates. This would prevent the desired further reduction of BDM to *p*-xylene, Table 3 shows the results obtained from catalysts screened for ester hydrogenation. Currently, complex **5**, Ru(MACHO)-BH, (carbonylhydrido(tetrahydroborato)[bis(2-diphenylphosphinoethyl)amino]ruthenium(II)), has shown the highest activity for PET depolymerization at 160 °C in a 1:1 mixture of THF:anisole, with an initial H_2

pressure of 40 atm (entry 13).[45] Complexes **6**, Ru(SNS), (dichlorotriphenylphosphine[bis(2-(ethylthio)ethyl)amine]ruthenium(II)), and **7**, Ru(PNN), (hydrochlorictriphenylphosphine[2-(diphenylphosphino)-N-(2-pyridinylmethyl)ethanamine]ruthenium(II)), showed very little activity for PET hydrogenation despite being known ester hydrogenation catalysts (entries 17-20).[46] Complex **7** was synthesized according to the literature[47], but all screenings with this complex were unable to hydrogenate PET. It is not clear why **6** and **7** did not work for our purposes, but could be due to a difference in either our samples of precatalysts or in our reaction techniques.

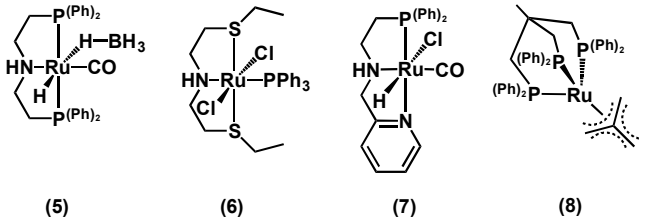

(5) (6) (7) (8)

Figure 2.7 Previously reported ester hydrogenation catalysts were screened in this work.

Complex **8**, Ru(triphos)-TMM, (triphos = 1,1,1-tris(diphenylphosphinomethyl)ethane, TMM = trimethylene methane), was then trialed as it is a known example of an acid stable ester hydrogenation catalyst, Table 2.[48] Initial hydrogenation trials with **8** showed promise, but it was unable to achieve the same % yield as **5** (entries 12 & 21). Additionally, unidentified product(s) were observed with signals at 167.8, 165.9, 156.9, 134.7, 126.9, 60.6, 50.2, and 30.9 ppm in the ^{13}C NMR spectrum of the hydrogenation of PET with **8**, Figure 2.9. The Leitner group reported a higher % yield with **8** when an acid was added to the reaction. We decided to try adding 2 eq of $HNTf_2$ (trifluoromethanesulfonimide) to the

hydrogenation reaction with **8** (entry 20)[48] however, the TON and % yield of products decreased with the addition of $HNTf_2$. The amount of side products also decreased in this reaction, Figure 2.8, bottom spectrum. **8** was also trialed with an excess of H_2O (entry 23), but this dramatically reduced the TON and % conversion. This mirrors the reported reactivity for Ru(triphos)-TMM with esters, which have higher TON and % yield without added acid.[48] Finally, the reaction time was extended out to 120 hrs (entry 24), but the % conversion did not increase.

Table 3. PET hydrogenation results with known ester hydrogenation catalysts.

Entry	Precatalyst	$p(H_2)$/ atm	substrate (mmol)	catalyst (mmol)	base/acid additive (mmol)	TON (EG:BDM)	% Yield (EG:BDM)
12	**5**	40	1.60	0.03	n/a	46.3 : 47.2	89.8 : 91.6
13[a]	**5**	40	1.60	0.03	n/a	23.6 : 10.9	45.8 : 21.1
14	**5**	50	1.60	0.03	n/a	48.1 : 37.2	93.1 : 72.0
15	**5**	50	1.60	0.03	n/a	32.7 : 33.1	63.4 : 64.3
16	**6**	40	0.08	0.00	0.05 (KO*t*Bu)	0.0 : 0.0	0.0 : 0.0
17	**6**	40	0.08	0.00	0.05 (KO*t*Bu)	0.0 : 0.0	0.0 : 0.0
18	**7**	50	0.09	0.00	0.15 (KO*t*Bu)	0.0 : 0.0	0.0 : 0.0
19	**7**	50	0.08	0.00	0.02 (KO*t*Bu)	0.0 : 0.0	0.0 : 0.0
20	**8**	50	1.60	0.02	0.04 ($HNTf_2$)	19.0 : 5.9	28.2 : 8.8
21	**8**	50	1.60	0.02	none	47.5 : 26.1	70.4 : 38.7
22	**8**	80	1.60	0.02	none	----	----
23[b]	**8**	50	1.61	0.02	none	0.0 : 3.6	0.0 : 5.3
24[c]	**8**	50	1.60	0.02	none	51.2 : 28.6	75.7 : 42.2

[a] Just anisole was used as the solvent. [b] 200 µL H_2O was added to the reaction. [c] Reaction time extended out to 120 h.

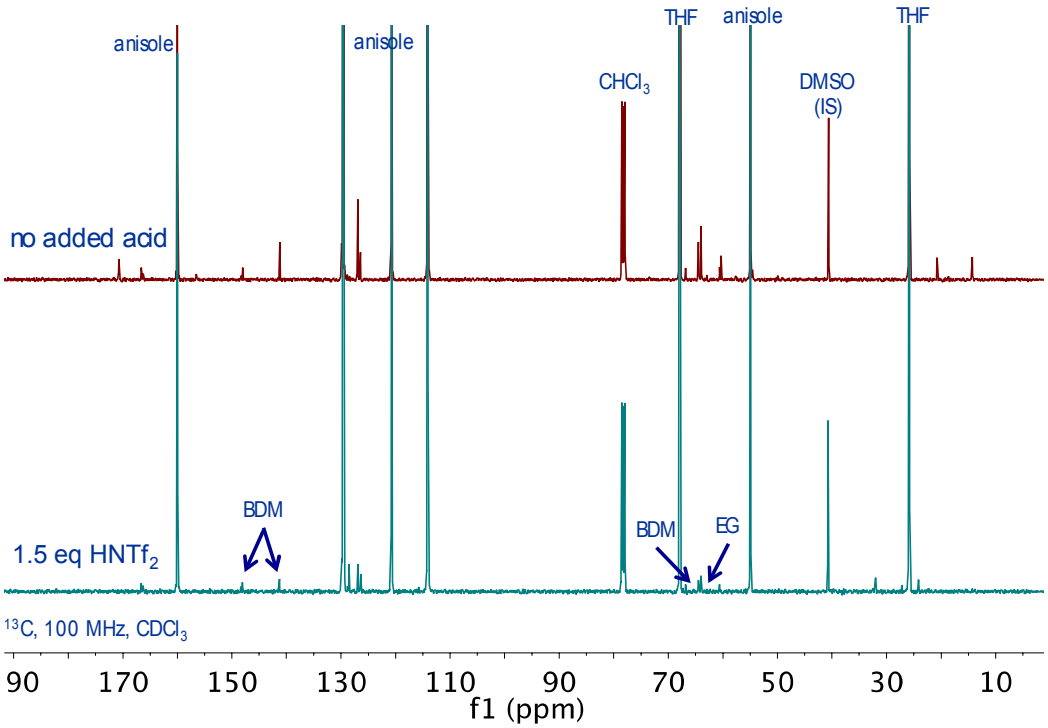

Figure 2.8 ^{13}C NMR spectrum of PET hydrogenation with **4**.

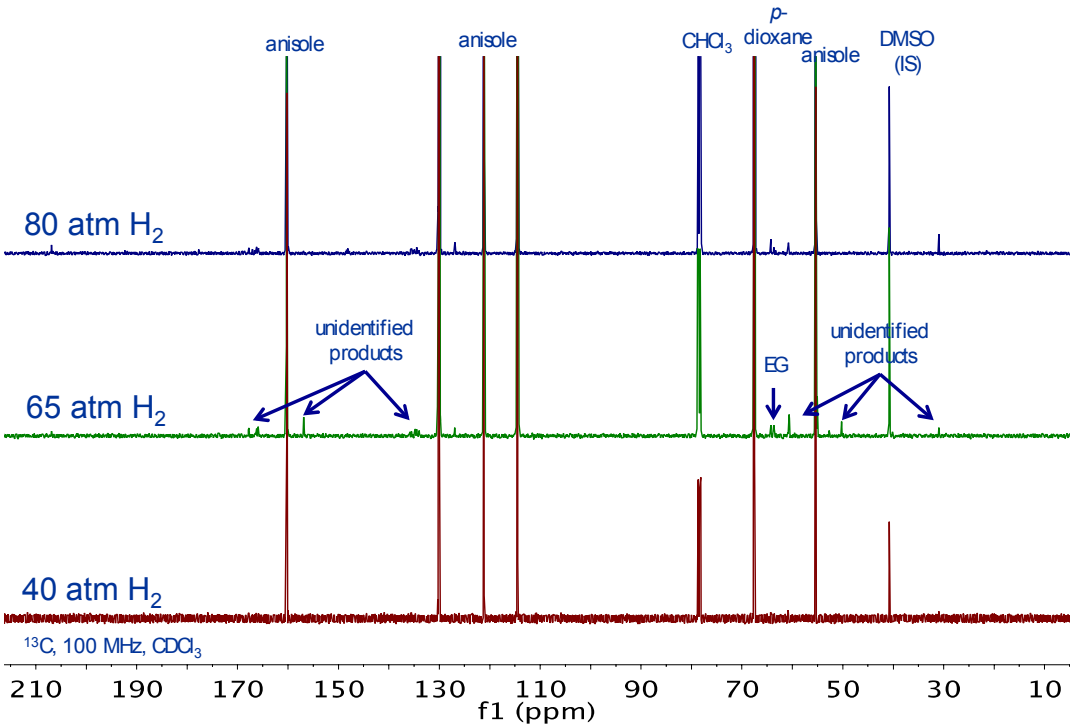

Figure 2.9 ^{13}C NMR spectrum of PET hydrogenation with **4** at 40, 65, and 80 atm of H_2.

2.4 Alcohol deoxygenation:

Partial deoxygenation of glycerol to give 1,3-propanediol and 1-propanol were previously demonstrated with an Ir(POCOP)$^{t\text{Bu}4}$(CO) catalyst.[49] Complex **1** (Ir(POCOP)$^{i\text{Pr}4}$H(CO)Cl) and was chosen because it has a less sterically hindered active site due to replacement of the *tert*-butyl with isopropyl substituents.[50] Benzyl alcohol was chosen as a model substrate for deoxygenation as toluene would be an easily identifiable product by ^{1}H NMR spectroscopy. Preliminary trials with **1** demonstrate the reduction of benzyl alcohol to toluene is possible, Figure 2.10. The acid content for alcohol deoxygenation was increased from 0.2 M, used for ester hydrogenation, to 1.0M. A 0.25% catalyst loading was also used. The reaction mixture was then heated to 200 °C under 80 atm of H_2 for 24 hours, and a TON of 43.3 and toluene yield of 10.8% was observed by ^{1}H NMR spectroscopy. The observation of toluene product in this reaction shows promise for the deoxygenation of BDM. Next, BDM deoxygenation was trialed with **1** under similar conditions. A lower acid content of 0.2 M H_2SO_4 was used for the reaction since it was the acid concentration initially used in the glycerol project.[49] A TON of 5.0 and 0.1 % yield of *p*-xylene was observed by ^{1}H NMR spectroscopy, which demonstrates diol deoxygenation is possible with **1** under acidic conditions. It is possible that increasing the acid content could increase the TON and % yield.

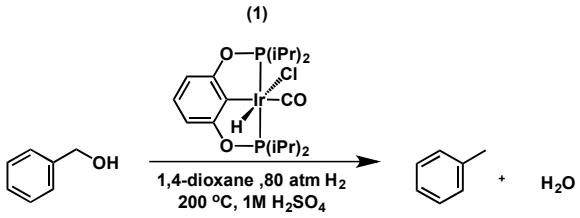

Figure 2.10 Ir(POCOP) deoxygenation complexes

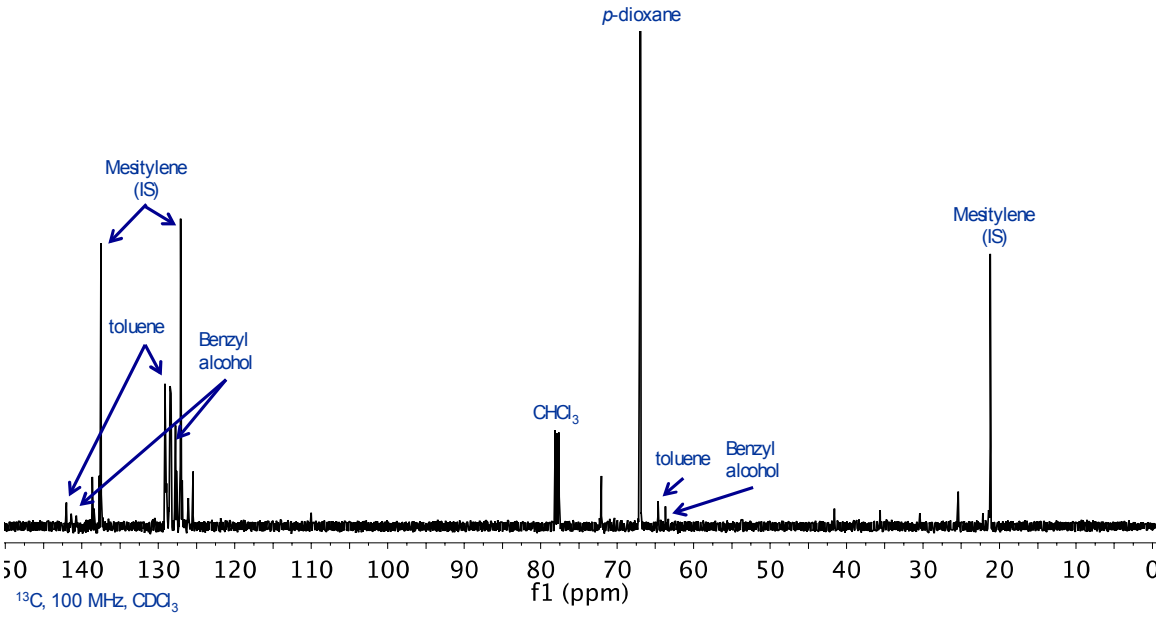

Figure 2.11 ^{13}C NMR spectrum of benzyl alcohol deoxygenation with **4**.

A catalytic cycle is proposed for the deoxygenation of BDM, which is based on the mechanism we proposed for glycerol deoxygenation, Figure 2.12.[49] Upon addition of hydrogen gas to **1** a dihydrogen complex is formed. This can act as a proton source for the protonation of BDM. Once the dihydride complex is formed it can then transfer a hydride to the protonated diol and reform the dihydrogen complex under an H_2 atmosphere.

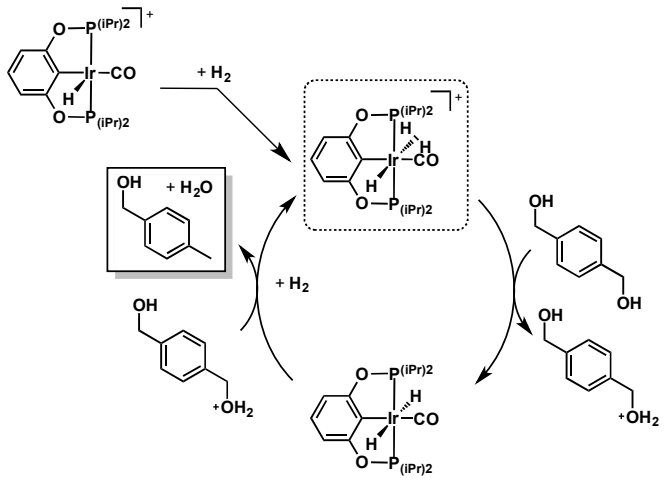

Figure 2.12 Proposed catalytic cycle for the hydrogenation of BDM.

One goal is to optimize the hydrogenation and deoxygenation catalysts to work together under the same experimental conditions. This will require trialing the catalysts proposed in Figure 2.7 for alcohol deoxygenation as well as ester hydrogenation. Increasing the concentration of H_2SO_4 should also be done to see if this increases the % conversion. Finally, other acids such as trifluoromethanesulfonic acid (HOTf) should be considered.

2.5 Summary:

In conclusion, the possibility of a tandem catalytic system for the depolymerization of PET was explored using hydrogenation and deoxygenation catalysts. Each component of this cycle has been tested for viability with model substrates. Hydrogenation of ethyl benzoate and deoxygenation of benzyl alcohol were assessed with an Ir(POCOP) catalyst, and both transformations are possible. More work is required to find the optimum catalyst and conditions for both of these transformations. Ru(MACHO)-BH afforded the highest TON and % yield for the hydrogenation of PET, but operates under basic conditions. Toluene was observed

from the deoxygenation of benzyl alcohol with **5,** Ru(MACHO)-BH. It is hoped that a tandem catalytic system can be found that is able to successfully hydrogenate PET and deoxygenate BDM efficiently.

In terms of future work on this project, the cationic complex [Ir(POCOP)^{iPr4}H(CO)]OTf (**2**) should be trialed for hydrogenation of ethyl benzoate and deoxygenation of benzyl alcohol as it is a proposed intermediate in the hydrogenation cycle, Figure 2.13.[49] One problem encountered with Ir(POCOP) catalyzed ester hydrogenation was low solubility of the precatalyst in polar solvents. Ir(POCOP)$^{t\text{Bu}4}$(NMe$_2$) (**3**) could be utilized as it is a known deoxygenation catalyst that requires a less complicated synthesis and has improved solubility in polar solvents.[49b]

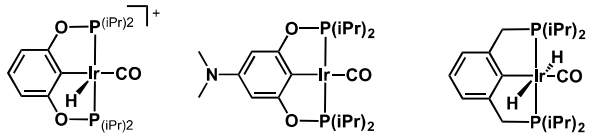

(2) (3) (4)

Figure 2.13 Ir(PCP) (left) and [Cp*Ir(bipy)H]OTf (left) catalyst

An extension of the project could also involve determining if catalytic hydrogenation of benzoic acid is possible with an Ir(POCOP) precatalyst. If this can be achieved then the products of acid catalyzed hydrolysis could be hydrogenated to benzyl alcohol and ethanol. From there deoxygenation of benzyl alcohol to toluene could be achieved.

Experimental:

General: Unless it is otherwise specified, all reactions involving metal complexes were carried out under a nitrogen atmosphere in a glove box, using standard Schlenk or high vacuum line techniques. Ir(POCOP)^{iPr4}H(CO)Cl[50], Ir(POCOP)^{iPr4}H$_2$(CO), and [Ir(POCOP)^{iPr4}H(CO)]OTf , Ru(SNS)[46], Ru(PNN)[47], Ru(triphos)-TMM[48] were prepared using previously reported literature procedures. Polyethylene terephthalate was cut from clear water bottles, and ground in a commercial grade food processor before use. Tetrahydrofuran (THF) used in synthetic procedures was passed through two packed columns of neutral alumina. Deuterated solvents ($CDCl_3$, tetrohydrofuran-d_8) were dried over sodium metal/benzophenone and distilled prior to use. All other reagents and solvents were used as received from their commercial suppliers unless otherwise specified. NMR spectra were recorded at 25 °C on a Bruker AV300, DRX499, AV500, or AV700 MHz spectrometer. All ^{1}H and ^{13}C NMR spectra are referenced to $SiMe_4$ (δ = 0 ppm) using the residual solvent signal as the internal standard and chemical shifts are reported in parts per million (ppm). Mesitylene and $CHCl_3$ were used as an internal standard for monitoring the ^{1}H NMR experiments. DMSO was used as an internal standard for monitoring the ^{13}C NMR experiments.

Reaction mixtures were quantified by collecting ^{13}C NMR spectra of neat reaction mixtures. A procedure for quantitative analysis of reaction mixtures was recently reported by Goldberg et al.[49b] Quantitative spectra were obtained by collecting inverse-gated decoupled NMR spectra to avoid NOE enhancement. To minimize integration problems associated with long relaxation times, delay times of

3 seconds were employed, and the paramagnetic additive $Cr(acac)_3$ (2.5 mg, 0.0072 mmol) was used as a relaxation agent.[51] DMSO was used as an internal standard.

Parr reactor experiments:

General procedure for ethyl benzoate hydrogenation with Ir(POCOP)^{iPr4}H(CO)Cl :

Hydrogenation reactions were carried out in Parr reactors outfitted with gas-inlet valves and pressure sensors. In a typical reaction, 45 mL reactors equipped with Teflon stir bars were charged with Ir(POCOP)^{iPr4}H(CO)Cl (7.76 mg, 0.013 mmol) and ethyl benzoate (780.9 mg, 5.2 mmol). Deionized water (0.197 g), dioxane (1.20 mL), and a sulfuric acid solution (1.0 M) was added with a micropipette (52 µL, 0.052 mmol). Reactors were stirred at 400 rpm, purged with H_2 for 4 min, pressurized to 80 bar, and heated to 200 °C over 20 min (pressure increases to 110 bar). After 48 h, the reactor was allowed to cool to room temperature and then cooled in an ice water bath for 20 min before venting slowly. DMSO (220 mg, 2.82 mmol) was then added to the reactor as an internal standard, and 0.4 mL of the reactor sample was then placed in a NMR tube with $CDCl_3$. The sample was analyzed by inverse-gated ^{13}C NMR spectroscopy.

General procedure for deoxygenation with Ir(POCOP)^{iPr4}H(CO)Cl :

Deoxygenation reactions were carried out in Parr reactors outfitted with gas-inlet valves and pressure sensors. In a typical reaction, 45 mL reactors equipped with Teflon stir bars were charged with Ir(POCOP)^{iPr4}H(CO)Cl (7.76 mg, 0.013 mmol) and benzyl alcohol (562.3 mg, 5.2 mmol). Dioxane (1.20 mL), and a sulfuric acid solution (1.0 M) was added with a micropipette (0.197 mL, 0.052 mmol).

Reactors were stirred at 400 rpm, purged with H_2 for 4 min, pressurized to 80 bar, and heated to 200 °C over 20 min (pressure increases to 110 bar). After 48 h, the reactor was allowed to cool to room temperature and then cooled in an ice water bath for 20 min before venting slowly. DMSO (220 mg, 2.82 mmol) was then added to the reactor as an internal standard, which was then placed in a NMR tube with $CDCl_3$. The sample was analyzed by inverse-gated ^{13}C NMR spectroscopy.

---

[38] Karayannidis, G. P.; Achilias, D. S. *Macromol. Mater. Eng.* 2007, *292*, 128.
[39] H. Köpnick; M. Schmidt; W. Brügging; J. Rüter; W. Kaminsky (2005), "Polyesters", Ullmann's Encyclopedia of Industrial Chemistry A21, Weinheim: Wiley-VCH, pp. 233–238.
[40] Browne, M. A.; Crump, P.; Niven, S. J.; Teuten, E.; Tonkin, A.; Galloway, T.; Thompson, R. *Environ. Sci. Technol.*, **2011**, *45*, 9175–9179.
[41] Balaraman, E.; Gnanaprakasam, B.; Shimon, J., W., L.; Milstein, D. *J. Am. Chem. Soc.* **2010**, *132*, 16756-16758.
[42] Krall, E. M.; Klein, T. W.; Andersen, R. J.; Glasgow, R. W.; Reader, D. S.; Dauphinais, B. C.; McIlrath, S. P.; Fischer, A. A.; Carney, M. J.; Hudson, D. J.; Robertson, N. J. *Chem. Commun.* **2014**, *50*, 4884-4887.
[43] Choi, J.; MacArthur, A. H. R.; Brookhart, M.; Goldman, A. *Chem. Rev.* **2011**, 111, 1761-1779.
[44] Brewster, T. P.; Miller, A. J. M.; Heinekey, D. M.; Goldberg, K. I. *J. Am. Chem. Soc.* **2013**, 135, 16022-16025.
[45] Kuriyama, W.; Matsumoto, T.; Ogata, O.; Ino, Y.; Aoki, K.; Tanaka, S.; Ishida, K.; Kobayashi, T.; Sayo, N.; Saito, T. *Org. ProcessRes. Dev.* **2012**, *16*, 166-171.
[46] Spasyuk, D.; Smith, S.; Gusev, D. G. *Angew. Chem. Int. Ed.* **2013**, *52*, 2538-2542.
[47] Spasyuk, D.; Gusev, D. G. *Organometallics* **2012**, *31*, 5239-5242.
[48] Stein, T.; Meuresch, M.; Limper, D.; Schmitz, M.; Hölscher, M.; Coetzee, J.; Cole-Hamilton, D. J.; Klankermayer, J.; Leitner, W. *J. Am. Chem. Soc.* **2014**, *136*, 13217-13225.
[49] a) Folksey, T. J. A.; Heinekey, D. M.; Goldberg, K. I. *ACS Catal.* **2012**, *2*, 1285-1289. b) Lao, D. B.; Owens, A. C. E.; Heinekey, D. M.; Goldberg, K. I. *ACS Catal.* **2013**, *3*, 2391-2396.
[50] Goldberg, J. M.; Wong, G. W.; Brastow, K. E.; Kaminsky, W.; Goldberg, K. I.; Heinekey, D. M. *Organometallics* **2015**, *34*, 753–762.
[51] Lamar, G. N. Chem. Phys. Lett. **1971**, 10, 230–232.